© 2022. Published by The Company of Biologists Ltd | Development (2022) 149, dev200238. doi:10.1242/dev.200238

STEM CELLS AND REGENERATION

TECHNIQUES AND RESOURCES ARTICLE

A non-disruptive and efficient knock-in approach allows fate tracing of resident osteoblast progenitors during repair of vertebral lesions in medaka

Wen Hui Tan and Christoph Winkler*

ABSTRACT

During bone development and repair, osteoblasts are recruited to bone deposition sites. To identify the origin of recruited osteoblasts, cell lineage tracing using Cre/*loxP* recombination is commonly used. However, a confounding factor is the use of transgenic Cre drivers that do not accurately recapitulate endogenous gene expression or the use of knock-in Cre drivers that alter endogenous protein activity or levels. Here, we describe a CRISPR/Cas9 homology-directed repair knock-in approach that allows efficient generation of Cre drivers controlled by the endogenous gene promoter. In addition, a self-cleaving peptide preserves the reading frame of the endogenous protein. Using this approach, we generated *col10a1*$^{p2a\text{-}CreERT2}$ knock-in medaka and show that tamoxifen-inducible CreERT2 efficiently recombined *loxP* sites in *col10a1* cells. Similar knock-in efficiencies were obtained when two unrelated loci (*osr1* and *col2a1a*) were targeted. Using live imaging, we traced the fate of *col10a1* osteoblast progenitors during bone lesion repair in the medaka vertebral column. We show that *col10a1* cells at neural arches represent a mobilizable cellular source for bone repair. Together, our study describes a previously unreported strategy for precise cell lineage tracing via efficient and non-disruptive knock-in of Cre.

KEY WORDS: Lineage analysis, Bone repair, Homology-directed repair, *Col10a1*, *Col2a1a*, *Osr1*

INTRODUCTION

In bone remodeling and fracture repair, osteoclasts resorb old or damaged bone while osteoblasts synthesize mineralized matrix and mediate the formation of new bone (Einhorn and Gerstenfeld, 2015; Hadjidakis and Androulakis, 2006). Defects in the recruitment of osteoblasts to sites where bone formation is needed result in reduced bone density, increasing the risk of low bone mass disorders such as osteoporosis as well as leading to compromised fracture repair (Dirckx et al., 2013; Thiel et al., 2018). It has been shown that several chemotactic factors can guide the migration of osteoblasts and their progenitors (Colciago et al., 2009; Hengartner et al., 2013; Nakasaki et al., 2008; Otsuru et al., 2008). However, molecular and cellular mechanisms regulating the recruitment of osteoblasts to bone formation sites have not been completely elucidated (Bragdon and Bahney, 2018; Thiel et al., 2018). Identification of molecular cues driving osteoblast trafficking remains challenging, as the origin of recruited osteoblasts is not clearly defined (Bragdon and Bahney, 2018).

Zebrafish (*Danio rerio*) and medaka (*Oryzias latipes*) have been widely used as models in bone research (Lleras-Forero et al., 2019; Rosa et al., 2021; Tonelli et al., 2020). Components of the mineralized bone matrix are similar in teleosts and mammals (Lleras-Forero et al., 2019; Witten et al., 2017). In addition, molecular pathways governing differentiation of osteogenic cells are highly conserved (Valenti et al., 2020; Witten et al., 2017). We have previously generated transgenic medaka where inducible overexpression of receptor activator of NF-κB ligand (Rankl) leads to degradation of bone matrix in the medaka vertebral column (To et al., 2012). Subsequently, *collagen10a1* (*col10a1*)-expressing osteoblast progenitors accumulated at the bone lesion sites and differentiated into *osterix* (*osx*)-expressing mature osteoblasts, facilitating re-mineralization of induced lesions (Renn et al., 2013). The origin of these recruited *col10a1* osteoblast progenitors, however, remained unknown.

Cre/*loxP* recombination-mediated cell lineage tracing is a popular technique used to identify cellular sources contributing to tissue repair and regeneration (Dasyani et al., 2019; Fu et al., 2020; Geurtzen et al., 2014; Hu et al., 2017; Tu and Johnson, 2011). As Cre/*loxP* recombination is irreversible and heritable, all recombined cells and their progeny can be permanently labeled, allowing tracking of migration, proliferation and differentiation of cell lineages *in vivo* (Centanin et al., 2014; Livet et al., 2007; Pan et al., 2013). The precision of this approach depends highly on spatiotemporal control of Cre expression in the targeted population of cells (Song and Palmiter, 2018). In zebrafish and medaka, several transgenic Cre driver lines have been generated using either the Tol2 transposon system or I-SceI meganuclease (Dasyani et al., 2019; Knopf et al., 2011; Lee et al., 2014). However, these transgenesis approaches are limited as transgenes are often randomly integrated into the genome, potentially resulting in position effects and ectopic transgene expression (Kondrychyn et al., 2009; Thermes et al., 2002). For accurate cell lineage analyses, Cre driver lines are needed that recapitulate endogenous gene expression patterns with high fidelity. In zebrafish, two previous studies have reported the generation of endogenous Cre drivers by CRISPR/Cas9-mediated knock-in (Almeida et al., 2021; Kesavan et al., 2018). CRISPR/Cas9 was used to induce a site-specific double-stranded break in the genome and the inherent DNA repair mechanisms of the cell were exploited to insert CreERT2 into the endogenous gene loci (Almeida et al., 2021; Kesavan et al., 2018). However, these knock-in approaches resulted in a deleterious effect on the endogenous gene of interest, either reducing gene expression (Kesavan et al., 2018) or disrupting the gene-coding sequence (Almeida et al., 2021).

Department of Biological Sciences and Centre for Bioimaging Sciences, National University of Singapore, Singapore 117543, Singapore.

*Author for correspondence (dbswcw@nus.edu.sg)

W.H.T., 0000-0002-7576-3198; C.W., 0000-0003-4688-6241

Handling Editor: Ken Poss
Received 29 September 2021; Accepted 11 May 2022

Development (2022) 149, dev200238. doi:10.1242/dev.200238

Here, we therefore used a novel CRISPR/Cas9 knock-in approach to generate a medaka *col10a1* Cre driver line. A p2a linker was used for bicistronic expression of *col10a1* and a 4-hydroxytamoxifen (4-HT)-inducible *CreERT2*, and homology-directed repair (HDR) was used to replace the *col10a1* stop codon with a p2a-CreERT2 knock-in cassette. The knock-in cassette also included a *cardiac myosin light chain 2* (*cmlc2*):EGFP reporter, which allowed efficient screening of knock-in founders. To show reliability of this approach, we also knocked in p2a-CreERT2 with similar efficiencies at loci of two other genes, *odd-skipped related transcription factor 1* (*osr1*) and *collagen2a1a* (*col2a1a*). In mammals, *Col10a1* is expressed specifically in hypertrophic chondrocytes (Shen, 2005), while *col10a1* in teleosts is expressed in osteoblast progenitors, osteoblasts and chondrocytes (Eames et al., 2012; Renn et al., 2013; Renn and Winkler, 2012). Here, we show that *CreERT2* expression in *col10a1*$^{p2a\text{-}CreERT2}$ medaka recapitulated endogenous *col10a1* expression spatiotemporally. In addition, skeletal development and survivability were unaffected in both heterozygous and homozygous *col10a1*$^{p2a\text{-}CreERT2}$ medaka. By crossing *col10a1*$^{p2a\text{-}CreERT2}$ medaka with transgenic *loxP* reporter lines, we show that CreERT2 in *col10a1*$^{p2a\text{-}CreERT2}$ is functional and can be induced by 4-HT to catalyze efficient recombination and specific labeling of *col10a1*$^{+}$ cells in larvae and adult fins. Finally, using *col10a1*$^{p2a\text{-}CreERT2}$ cell labeling, we tracked the dynamics of *col10a1*$^{+}$ osteoblast progenitors after Rankl induction. We show that *col10a1*$^{+}$ osteoblast progenitors residing at neural arches are recruited to bone lesion sites in the vertebral centra where they contribute to re-mineralization. This identifies *col10a1*$^{+}$ cells as a resident source of osteoblasts that facilitate bone repair.

RESULTS

Generation of *col10a1*$^{p2a\text{-}CreERT2}$ medaka by CRISPR/Cas9-mediated homology-directed repair

To knock-in p2a-CreERT2 into the medaka *col10a1* locus, a CRISPR/Cas9-mediated homology-directed repair (HDR) strategy was used. A sequence positioned 37 base pairs (bp) upstream of the endogenous *col10a1* stop codon was selected as the knock-in target site for the guide RNA (gRNA) (Fig. 1, indicated in magenta). To facilitate HDR, a 292 bp sequence upstream and a 215 bp sequence downstream of the *col10a1* stop codon were cloned into the donor plasmid as 5′ and 3′ homology arms, respectively. These homology arms flank a 4.8 kb sequence, which consists of the p2a-CreERT2 coding sequence, as well as a secondary fluorescence reporter with a *cmlc2* promoter driving the expression of EGFP. At the 3′ ends of both EGFP and CreERT2, a stop codon and SV40 polyA (pA) signal were inserted. To prevent CRISPR/Cas9-cleavage at the *col10a1* gRNA site in the donor plasmid, PCR primers with template-primer mismatches were used to incorporate wobble bases (Fig. 1, magenta asterisks). Two mbait gRNA sites, previously reported to enhance knock-in efficiency (Kimura et al., 2014), were also included in the donor plasmid (Fig. 1).

To generate the *col10a1*$^{p2a\text{-}CreERT2}$ knock-in line, wild-type medaka embryos were injected with the donor plasmid, Cas9 nuclease, *col10a1* crRNA (targeting the *col10a1* gRNA site), mbait crRNA (targeting the mbait gRNA site) and tracrRNA at the one-cell stage (Fig. 2A). Injected F0 embryos were raised to 12 days post-fertilization (dpf) and screened for *cmlc2*:EGFP expression. Twenty-four out of 338 (7.1%) injected embryos showed mosaic *cmlc2*:EGFP expression and were raised as potential founders (Fig. 2B). Potential founders were out-crossed to wild-type fish and F1 progenies were screened for *cmlc2*:EGFP expression. Three out of seven (42.9%) potential founders transmitted the *cmlc2*:EGFP transgene to the next generation (Fig. 2B,C). To confirm precise knock-in at the *col10a1* locus, PCR was performed using a forward primer that binds to medaka genomic DNA at the *col10a1* locus and a reverse primer that binds to the donor plasmid (Fig. 1, yellow arrows, FP1, RP1). For *cmlc2*:EGFP-postive F1 offspring from two out of three potential founders, the expected 505 bp band was observed (Fig. 2B,D). Sequencing of the 505 bp amplicon revealed precise integration of the donor template into the *col10a1* locus at the 5′ homology region (Fig. 2E), identifying two *col10a1*$^{p2a\text{-}CreERT2}$ founders. Sequencing analysis also confirmed precise knock-in at the 3′ homology region (Fig. S1). Compared with wild-type, *col10a1*$^{p2a\text{-}CreERT2}$ medaka had single wobble base changes at the *col10a1* gRNA target site as expected (Fig. 2E, magenta asterisks). In addition, the endogenous *col10a1* stop codon was replaced with p2a-CreERT2;*cmlc2*:EGFP in-frame (Fig. 2E). Protein sequence prediction using the ExPaSy web tool

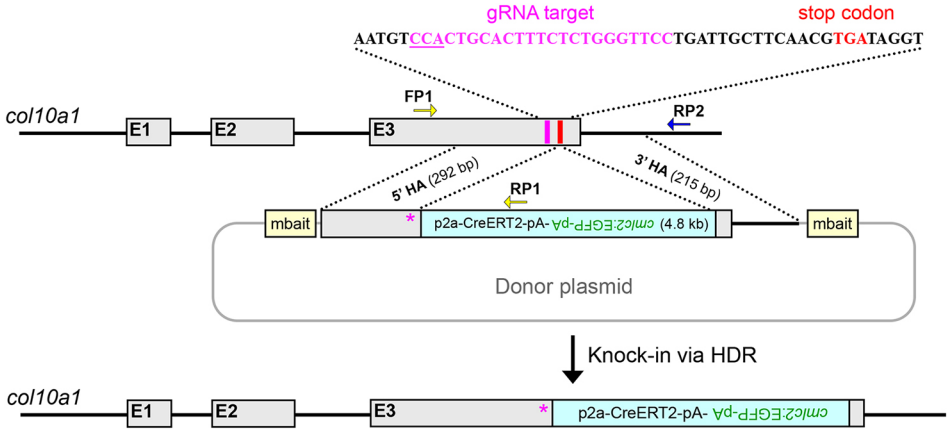

Fig. 1. Knock-in of p2a-CreERT2;*cmlc2*:EGFP into the medaka *col10a1* locus via CRISPR/Cas9-mediated homology-directed repair (HDR). Strategy for knock-in of p2a-CreERT2;*cmlc2*:EGFP into the *col10a1* locus. A donor plasmid containing two mbait guide RNA (gRNA) target sequences (yellow boxes) and two homology arms (5′ HA and 3′ HA, 292 bp and 215 bp, respectively) flanking the p2a-CreERT2;*cmlc2*:EGFP sequence (4.8 kb) was used. The *col10a1* gRNA target sequence is indicated in magenta and the protospacer adjacent motif (PAM) sequence is underlined. In the donor plasmid, wobble bases (magenta asterisks) were incorporated at the *col10a1* gRNA target sequence. The endogenous *col10a1* stop codon is indicated in red. Yellow arrows (FP1 and RP1) indicate PCR primers used for identification of precise knock-in at the 5′ homology region. Blue arrow (RP2) indicates reverse primer used for PCR genotyping of heterozygous and homozygous knock-in medaka. pA, polyA.

Development (2022) 149, dev200238. doi:10.1242/dev.200238

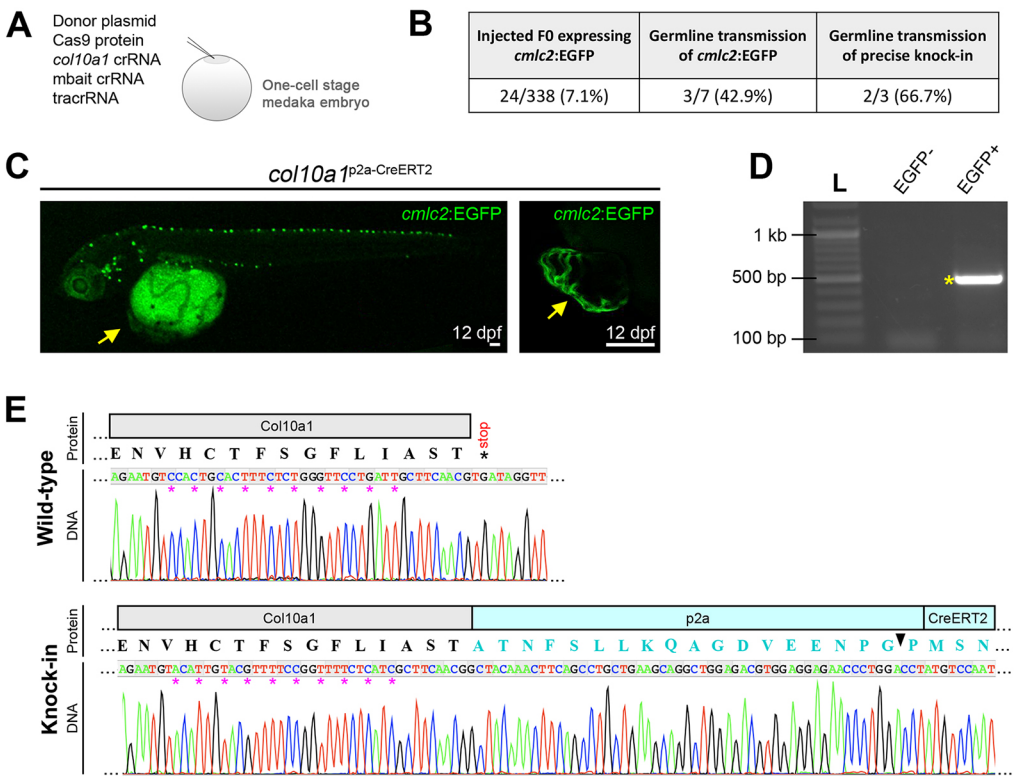

Fig. 2. Generation of *col10a1*$^{p2a\text{-}CreERT2}$ knock-in medaka. (A) For generating the knock-in line, a solution containing the donor plasmid, Cas9 nuclease, *col10a1* crRNA, mbait crRNA and tracrRNA was injected into one-cell stage wild-type medaka embryos. (B) Table showing the efficiency of knock-in and germline transmission. (C) Live confocal imaging showing *cmlc2*:EGFP expression in the heart (yellow arrows) of a *col10a1*$^{p2a\text{-}CreERT2}$ F1 larva at 12 dpf. Left image shows a *z*-stack overview. Right image shows a 2D magnified view of the heart. Both images show the lateral view. Scale bars: 100 µm. (D) DNA agarose gel showing PCR-genotyping of a *cmlc2*:EGFP-positive (EGFP+) F1 larva and its *cmlc2*:EGFP-negative (EGFP-; control) sibling. Yellow asterisk indicates the expected 505 bp band. L, DNA ladder. (E) DNA sequencing analysis and the predicted amino acid sequence of Col10a1 at the 5′ homology region in wild-type and *col10a1*$^{p2a\text{-}CreERT2}$ knock-in medaka. Magenta asterisks indicate bases that were wobbled in *col10a1*$^{p2a\text{-}CreERT2}$. Black arrowhead indicates the p2a self-cleavage site. Black asterisk indicates the endogenous *col10a1* stop codon.

(Swiss Institute of Bioinformatics; SIB) revealed that the amino acid sequence of Col10a1 in *col10a1*$^{p2a\text{-}CreERT2}$ medaka remains undisrupted until immediately before its endogenous stop codon (Fig. 2E).

To demonstrate the reproducibility of our knock-in approach, we used the same strategy for a targeted knock-in of p2a-CreERT2 at the *osr1* (Fig. S2A) and *col2a1a* (Fig. S3A) gene loci. Thirteen out of 138 injected embryos (9.4%) and 10 out of 122 injected embryos (8.2%) showed mosaic *cmlc2*:EGFP expression at 12 dpf for *osr1* and *col2a1a*, respectively (Figs S2B, S3B). To confirm precise knock-in at the *osr1* and *col2a1a* loci, *cmlc2*:EGFP-positive F0 larvae were fin clipped at 12 dpf for PCR genotyping and DNA sequencing analysis. Correct knock-in sequences were detected in four out of 13 *cmlc2*:EGFP-positive F0 (30.8%) and three out of 10 *cmlc2*:EGFP-positive F0 (30.0%) for *osr1* and *col2a1a*, respectively (Figs S2C-D, S3C-D). These findings show that our knock-in approach is an effective and efficient method for generating knock-ins with precise integration.

CreERT2 expression in *col10a1*$^{p2a\text{-}CreERT2}$ knock-in medaka recapitulates *col10a1* expression

For accurate cell fate and lineage analyses, it is important that Cre driver lines recapitulate endogenous gene expression patterns spatiotemporally. We previously generated *col10a1*:CreERT2-p2a-mCherry transgenic medaka and showed that the transgene expression matched endogenous *col10a1* expression in the adult medaka fin (Dasyani et al., 2019). However, in the larval vertebral column, the *col10a1*:CreERT2-p2a-mCherry transgene is ectopically expressed (Fig. S4). Hence, the *col10a1*:CreERT2-p2a-mCherry transgenic line is not suitable for lineage tracing of *col10a1* osteoblast progenitors in the vertebral column. To test whether *CreERT2* transcription in *col10a1*$^{p2a\text{-}CreERT2}$ knock-in medaka recapitulates endogenous *col10a1* transcription, whole-mount RNA *in situ* hybridization was performed with a *CreERT2* riboprobe and compared with *col10a1* expression in wild-type medaka at 5, 7 and 9 dpf (Fig. 3A-B″′). At all three stages, *CreERT2* expression was identical to *col10a1* expression. At 5 dpf, both *col10a1* and *CreERT2* expression were observed in intramembranous bones such as the parasphenoid, cleithrum, operculum and branchiostegal ray (Fig. 3A,B). At 7 dpf, in addition to intramembranous bones, *col10a1* and *CreERT2* were also expressed in the ceratohyal, which is a chondral bone (Fig. 3A′, B′). At 9 dpf, *col10a1* and *CreERT2* expression were detected in cartilage structures such as the ceratobranchials (Fig. 3A″,B″). Similar *col10a1* and *CreERT2* expression patterns were also observed in neural arches and vertebral bodies of the vertebral column, as well as in the hypural and fin rays of the caudal fin (Fig. 3A″′,B″′; *CreERT2* sense control in Fig. S5).

Next, to examine whether CreERT2 protein is expressed specifically in *col10a1* cells, the *col10a1*$^{p2a\text{-}CreERT2}$ line was crossed to a previously established *col10a1*:GFP transgenic line (Renn et al., 2013) and CreERT2 immunohistochemistry was performed on 20 µm transverse cryosections of the 9 dpf vertebral column (position indicated by the red dotted line in Fig. 3B″′;

Development (2022) 149, dev200238. doi:10.1242/dev.200238

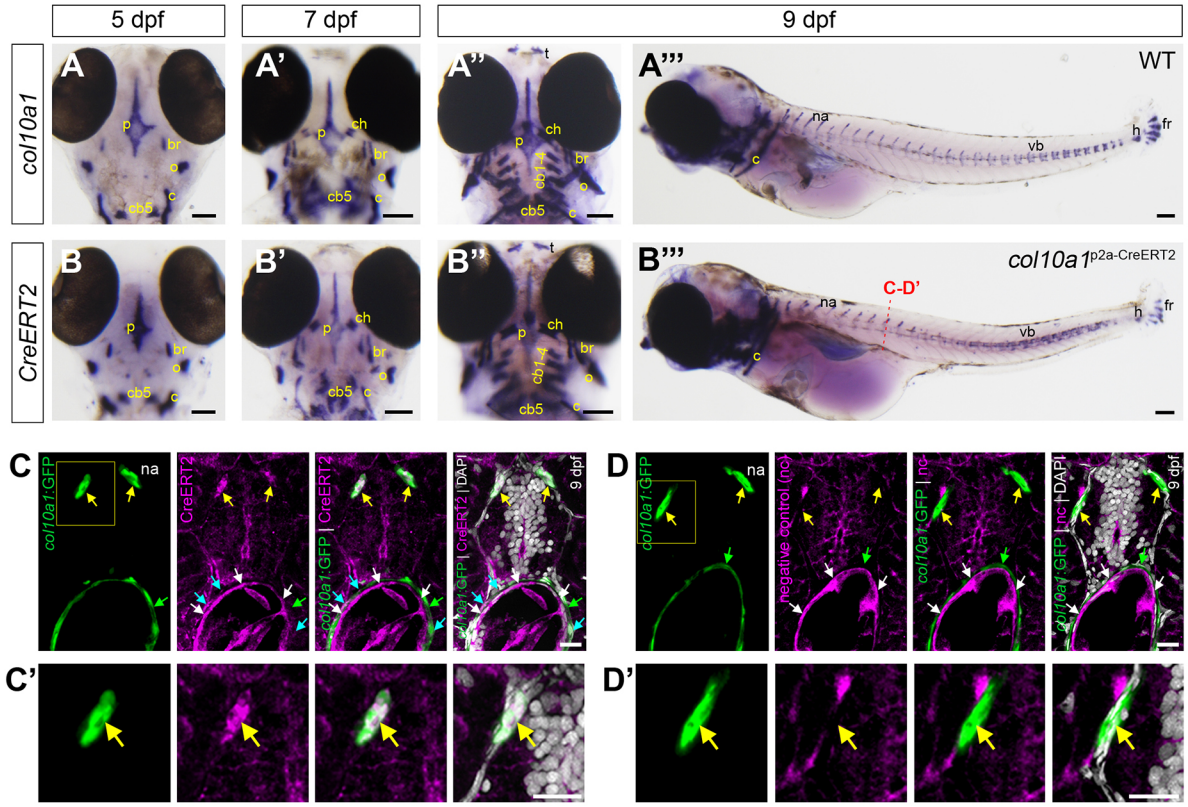

Fig. 3. Expression of *CreERT2* in *col10a1*$^{p2a\text{-}CreERT2}$ medaka recapitulates endogenous *col10a1* expression. (A-B‴) Whole-mount RNA *in situ* hybridization of *col10a1* in wild-type medaka (A-A‴) and *CreERT2* in *col10a1*$^{p2a\text{-}CreERT2}$ medaka (B-B‴). Similar *col10a1* and *CreERT2* expression patterns were observed at 5 dpf (A,B), 7 dpf (A′,B′) and 9 dpf (A″,A‴,B″,B‴). Ventral views: A-A″,B-B″. Lateral views: A‴,B‴. Red dotted line in B‴ indicates region of the vertebral column used to obtain transverse cryosections shown in C-D′. (C-D′) Confocal images showing Cre immunostaining (C,C′) and negative control (D,D′) on 20 µm transverse cryosections of the vertebral column in *col10a1*$^{p2a\text{-}CreERT2}$|*col10a1*:GFP larvae at 9 dpf. DAPI was used to stain the nuclei. Yellow arrows indicate the neural arches. White arrows indicate the centrum of the vertebral body. Green arrows indicate *col10a1*:GFP cells at the vertebral centra. Cyan arrows indicate cells at the vertebral centra co-expressing CreERT2 and *col10a1*:GFP. Yellow boxes in C and D indicate magnified views, as shown in C′ and D′, respectively. br, branchiostegal ray; cb1-5, ceratobranchials 1-5; ch, ceratohyal; c, cleithrum; fr, fin ray; h, hypural; na, neural arch; o, operculum; p, parasphenoid; t, teeth; vb, vertebral body. Scale bars: 100 µm in A-B‴; 15 µm in C-D′.

Fig. 3C-D′). Similar to *col10a1* and *CreERT2* expression patterns in the vertebral column (Fig. 3A‴,B‴), CreERT2 protein was detected at neural arches (Fig. 3C,C′, yellow arrows). In addition, at the neural arches, CreERT2 protein expression overlapped with *col10a1*:GFP expression (Fig. 3C,C′, yellow arrows). In contrast, no staining was observed in neural arches in negative controls (Fig. 3D,D′, yellow arrows). In both CreERT2 staining and negative controls, non-specific staining was observed at the mineralized matrix of vertebral centra (Fig. 3C,D, white arrows) and *col10a1*:GFP expression was observed in cells lining the mineralized matrix (Fig. 3C,D, green arrows). CreERT2 was detected in a subset of *col10a1*:GFP cells lining the mineralized matrix (Fig. 3C, cyan arrows). This is in line with low endogenous expression levels of *col10a1* and *CreERT2* at the vertebral centra, as shown in Fig. 3A‴ and Fig. 3B‴, respectively. Together, this shows that *CreERT2* expression in *col10a1*$^{p2a\text{-}CreERT2}$ medaka faithfully recapitulates endogenous *col10a1* expression at both the RNA and protein level.

col10a1$^{p2a\text{-}CreERT2}$ knock-in medaka have normal bone and cartilage development

In knock-in fish, nucleotide changes were created at the *col10a1* gRNA target site and p2a was used to link the *col10a1*- and *CreERT2*-coding sequences (Fig. 2E). P2a is a 19 amino acid linker that self-cleaves between glycine and proline at its C-terminal end during translation (Donnelly et al., 2001). In *col10a1*$^{p2a\text{-}CreERT2}$ medaka, the p2a self-cleavage is predicted to result in Col10a1 having 18 additional amino acids at its C-terminal end and CreERT2 having an additional proline residue at its N-terminal end (Fig. 2E, black arrowhead indicates p2a cleavage site). To test whether alterations at the C-terminal end of Col10a1 result in any deleterious effects on protein function, we had previously generated a medaka mutant with a 5 bp deletion at the *col10a1* gRNA site, leading to a frameshift of the last 11 amino acids and elongation of its protein by one amino acid (W.H.T. and C.W., unpublished; Fig. 1, *col10a1* gRNA site indicated in magenta). Heterozygous *col10a1* medaka mutants exhibited aberrant skeletal formation, while homozygous mutants had severe bone and cartilage defects, and did not survive beyond 4 weeks (W.H.T. and C.W., unpublished; Fig. 4A). This suggests that distinct alterations at the C-terminal end of Col10a1 can principally result in severe skeletal defects. To elucidate whether the specific nucleotide alterations and additional 18 amino acids introduced in *col10a1*$^{p2a\text{-}CreERT2}$ medaka had any effect on skeletal development, Alizarin Red bone staining and Alcian Blue cartilage staining were performed on heterozygous [wild type (WT)/knock-in (KI)] and homozygous (KI/KI) *col10a1*$^{p2a\text{-}CreERT2}$ medaka and compared with homozygous *col10a1* medaka mutants (Mut/Mut) (Fig. 4A,B). Genotyping of WT/KI and KI/KI medaka was performed by multiplex PCR using three primers, as indicated in Fig. 1 (FP1, RP1 and RP2 in Fig. 1; Fig. S6). In the vertebral column at 12 dpf, mineralized neural arches were absent in

Development (2022) 149, dev200238. doi:10.1242/dev.200238

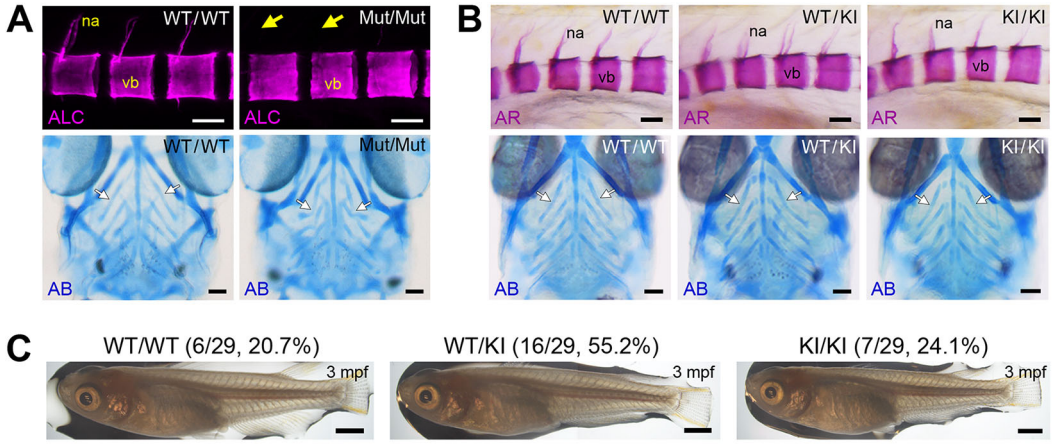

Fig. 4. Bone and cartilage formation are unaffected in *col10a1*$^{p2a\text{-}CreERT2}$ knock-in medaka. (A) Bone and cartilage staining by Alizarin complexone (ALC, top panel) and Alcian Blue (AB, bottom panel), respectively, in 12 dpf homozygous *col10a1* medaka mutants (Mut/Mut) and wild-type siblings (WT/WT). Neural arches were missing (yellow arrows) and ceratobranchials (white arrows) were deformed in Mut/Mut larvae compared with wild-type siblings. (B) Bone and cartilage staining by Alizarin Red (AR, top panel) and Alcian Blue (AB, bottom panel), respectively, in 12 dpf heterozygous *col10a1*$^{p2a\text{-}CreERT2}$ (WT/KI), homozygous *col10a1*$^{p2a\text{-}CreERT2}$ (KI/KI) and WT siblings (WT/WT). No skeletal defects were observed in WT/KI and KI/KI larvae. na, neural arch; vb, vertebral body. (C) Bright-field images of 3 mpf WT/KI, KI/KI and WT/WT siblings from an in-cross of WT/KI carriers. Ratio of WT/WT:WT/KI:KI/KI was found to be 6:16:7. Fins were clipped for genotyping. No morphological differences were observed for all three genotypes. Scale bars: 50 µm in A,B; 1 mm in C.

Mut/Mut larvae when compared with WT/WT controls (Fig. 4A, top panel, yellow arrows). On the other hand, mineralized neural arches formed normally in WT/KI and KI/KI larvae compared with WT/WT controls (Fig. 4B, top panel). In addition, Alcian Blue staining at 12 dpf showed that ceratobranchials were deformed in Mut/Mut larvae compared with WT/WT controls (Fig. 4A, bottom panel, white arrows). In contrast, no deformities were observed in ceratobranchials of WT/KI and KI/KI larvae compared with WT/WT controls (Fig. 4B, bottom panel, white arrows). Alizarin Red and Alcian Blue staining also showed that other skeletal structures where *col10a1* is expressed, such as the branchiostegal rays, cleithrum, hypural and fin rays (Fig. 3), formed normally in WT/KI and KI/KI larvae compared with WT/WT controls (Fig. S7). At adult stage (3 months post-fertilization; mpf), no phenotypic abnormalities were observed in WT/KI and KI/KI fish compared with WT/WT controls (Fig. 4C). In addition, compared with *col10a1* Mut/Mut medaka in which lethality was observed at 1 mpf (T.W.H. et al., unpublished), genotyping of 3 mpf offspring from an in-cross of WT/KI carriers revealed a ratio of 6 WT/WT (20.7%):16 WT/KI (55.2%):7 KI/KI (24.1%; Fig. 4C), which is close to a 1:2:1 Mendelian ratio. Together, this indicates that the integration of p2a-CreERT2;*cmlc2*:EGFP at the medaka *col10a1* locus was non-disruptive and did not impair skeletal development or survivability. Hence, the *col10a1*$^{p2a\text{-}CreERT2}$ knock-in line is suitable for cell lineage analyses during skeletal development and repair in medaka.

Inducible Cre/*loxP* recombination for mosaic labeling of *col10a1* cells in *col10a1*$^{p2a\text{-}CreERT2}$ medaka crossed to *loxP* reporters

To test whether CreERT2 in *col10a1*$^{p2a\text{-}CreERT2}$ medaka can be induced to catalyze recombination between *loxP* sites in *col10a1* cells, the *col10a1*$^{p2a\text{-}CreERT2}$ line was crossed to two transgenic *loxP* reporter lines, GaudiRSG and GaudiBBW2.1, respectively (Fig. 5A; Centanin et al., 2014). In GaudiRSG, DsRed fluorescent protein is ubiquitously expressed by default and can be switched to nuclear localized nlsEGFP upon Cre/*loxP* recombination (Fig. 5A; Centanin et al., 2014). In GaudiBBW2.1, default membrane-tagged ECFP expression can be switched to either dTomato, YFP or nlsEGFP expression upon Cre/*loxP* recombination (Fig. 5A; Centanin et al., 2014). For induction of CreERT2 activity, double heterozygous *col10a1*$^{p2a\text{-}CreERT2}$|GaudiRSG or *col10a1*$^{p2a\text{-}CreERT2}$|GaudiBBW2.1 embryos were treated with 4-hydroxytamoxifen (4-HT; 10 µM; 6 h) at 9 dpf, when *col10a1* is expressed in bone and cartilage cells (Fig. 3A″,A″′). After 4-HT treatment, Cre/*loxP* recombination-mediated cell labeling was observed in a pattern in line with *col10a1* expression (Fig. 5B-G). One day post 4-HT treatment (dp4HT), Cre/*loxP* recombination-mediated fluorescent reporter switching was observed in subsets of chondrocytes (Fig. 5B,C, white arrows) and perichondral osteoblasts (Fig. 5B, B′, yellow arrows) at the ceratohyal. At 7 dp4HT, a switch in fluorescent reporter expression was observed in cells lining the neural arches (Fig. 5D,E, white arrows) and vertebral bodies (Fig. 5D,E, yellow arrows) in the vertebral column. These cell labeling patterns matched endogenous *col10a1* expression (Fig. 3A″,A″′) as well as GFP expression in the *col10a1*:GFP transgenic line, which marks all *col10a1*-expressing cells (Renn et al., 2013; Fig. 5F,G). For *col10a1*$^{p2a\text{-}CreERT2}$|GaudiRSG and *col10a1*$^{p2a\text{-}CreERT2}$|GaudiBBW2.1, Cre/*loxP* recombination-mediated cell labeling was observed in 22 out of 36 (61.1%) and 12 out of 21 (57.1%) 4-HT-treated embryos, respectively. To test whether higher rates of Cre/*loxP* recombination can be achieved with the *col10a1*$^{p2a\text{-}CreERT2}$ line, we extended the 4-HT treatment (at 10 µM) of double heterozygous *col10a1*$^{p2a\text{-}CreERT2}$|GaudiRSG embryos from 6 to 24 h at 9 dpf. Under these conditions, 20 out of 20 (100%) 4-HT-treated embryos showed Cre/*loxP* recombination-labeled *col10a1* cells in the vertebral column at 13 dpf (Fig. 5H). Compared with *col10a1*:GFP, where 54±3 cells were labeled per vertebral body (Fig. 5I, K; n=7 fish, 3 vertebral bodies per fish), 31±5 cells (57.4%) were labeled in the vertebral body of 4-HT-treated *col10a1*$^{p2a\text{-}CreERT2}$|GaudiRSG larvae at 13 dpf (Fig. 5H,K; n=7 fish, 3 vertebral bodies per fish). In addition, no cell labeling was observed in larvae not treated with 4-HT (>100 larvae each for GaudiRSG and GaudiBBW2.1), indicating that Cre/*loxP* recombination did not occur in the absence of 4-HT. This shows that CreERT2 in *col10a1*$^{p2a\text{-}CreERT2}$ medaka is functional, non-leaky and, depending on the treatment duration of 4-HT, can catalyze different rates of recombination between *loxP* sites for specific labeling of *col10a1* cells.

Development (2022) 149, dev200238. doi:10.1242/dev.200238

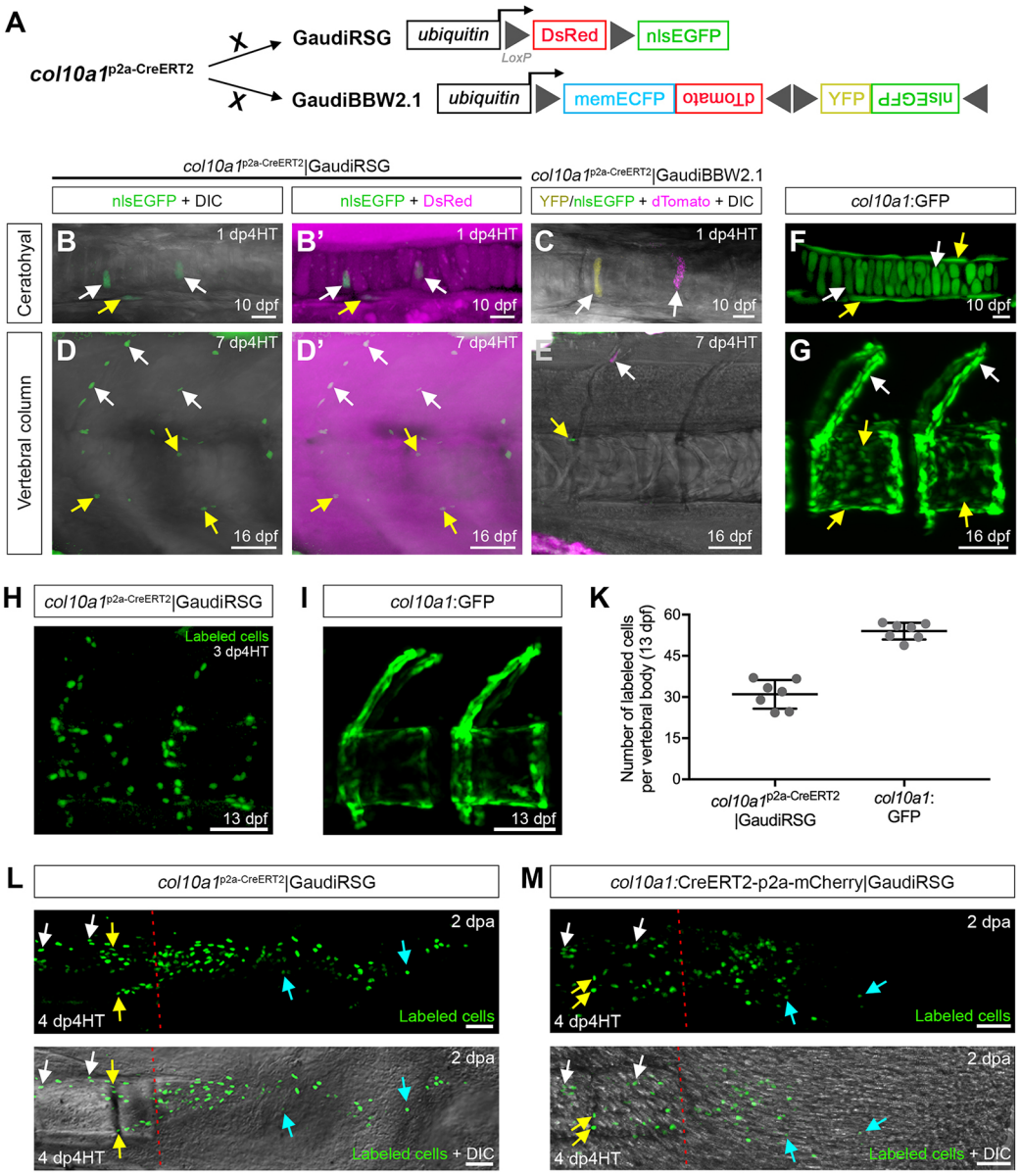

Fig. 5. Inducible Cre/*loxP* recombination and *col10a1* cell labeling in *col10a1*$^{p2a\text{-}CreERT2}$ knock-in medaka crossed to transgenic *loxP* reporter lines. (A) *col10a1*$^{p2a\text{-}CreERT2}$ knock-in medaka were crossed to either GaudiRSG or GaudiBBW2.1, which are transgenic *loxP* reporter lines where floxable fluorescent reporters are expressed under the control of a ubiquitin promoter. (B-E) Confocal images showing Cre/*loxP* recombination-mediated switch in fluorescent reporter expression in subsets of *col10a1* cells after 4-HT treatment in *col10a1*$^{p2a\text{-}CreERT2}$|GaudiRSG (B,B′,D,D′) and *col10a1*$^{p2a\text{-}CreERT2}$|GaudiBBW2.1 larvae (C,E). Labeling was observed in chondrocytes (white arrows, B-C) and perichondral osteoblasts (yellow arrows, B,B′) at the ceratohyal, as well as in osteoblast progenitors at the neural arches (white arrows, D,E) and vertebral bodies (yellow arrows, D,E) at the vertebral column. dp4HT, days post 4-hydroxytamoxifen treatment. (F,G) Confocal images showing *col10a1*:GFP expression in ceratohyal chondrocytes (white arrows, F) and perichondral osteoblasts (yellow arrows, F), as well as osteoblast progenitors at the neural arches (white arrows, G) and vertebral bodies (yellow arrows, G) at the vertebral column. (H-K) Determination of *col10a1* cell labeling capacity in the vertebral column of *col10a1*$^{p2a\text{-}CreERT2}$|GaudiRSG larvae at 3 dp4HT. Number of nlsEGFP-labeled cells in vertebral column of *col10a1*$^{p2a\text{-}CreERT2}$|GaudiRSG larvae (H) was compared with the number of GFP-positive cells in the vertebral column of *col10a1*:GFP larvae (I). (K) *n*=7 larvae, 3 VB per larvae. Data are mean±s.d. (L,M) Confocal images showing nlsEGFP-labeled cells in the regenerating fin of *col10a1*$^{p2a\text{-}CreERT2}$|GaudiRSG (L) and *col10a1*:CreERT2-p2a-mCherry|GaudiRSG (M) adult fish (5 months old) at 2 days post-amputation (dpa) and 4 dp4HT. Red dotted lines indicate the amputation plane. Yellow arrows indicate joint cells. White arrows indicate fin segmental osteoblasts. Cyan arrows indicate cells in the blastema. Scale bars: 10 µm in B-C,F; 50 µm in D-E,G-I,L,M.

We previously used *col10a1*:CreERT2-p2a-mCherry transgenic medaka for lineage tracing of *col10a1* cells in the regenerating adult fin and showed that labeled *col10a1* cells migrate beyond the amputation plane, contributing to blastema formation and fin regeneration (Dasyani et al., 2019). To test whether the *col10a1*$^{p2a\text{-}CreERT2}$ line is also functional at adult stages for cell lineage analyses, we performed lineage tracing of *col10a1* cells in the regenerating adult fin of *col10a1*$^{p2a\text{-}CreERT2}$|GaudiRSG knock-in medaka. Similar to transgenic *col10a1*:CreERT2-p2a-mCherry|GaudiRSG medaka, Cre/*loxP* recombination-mediated cell labeling was observed specifically in joint cells and osteoblasts proximal to the amputation plane in *col10a1*$^{p2a\text{-}CreERT2}$|GaudiRSG knock-in medaka (Fig. 5L,M, yellow and white arrows). In addition, in 2 dpa regenerates of both *col10a1*$^{p2a\text{-}CreERT2}$|GaudiRSG and *col10a1*:

Development (2022) 149, dev200238. doi:10.1242/dev.200238

CreERT2-p2a-mCherry|GaudiRSG fins, labeled cells were observed in the blastema (Fig. 5L,M, cyan arrows), indicating that labeled *col10a1* cells contribute to fin regeneration. Together, this shows that the *col10a1*$^{p2a\text{-}CreERT2}$ line can be used for *col10a1* cell fate and lineage analyses at both larval and adult stages.

Resident *col10a1* osteoblast progenitors at neural arches are recruited to bone repair sites after Rankl induction

We previously generated *rankl*:HSE:CFP transgenic medaka and showed that, upon heat-shock, ectopic expression of Rankl led to excessive formation of osteoclasts and the formation of osteoporotic lesions in the mineralized matrix of the vertebral column (To et al., 2012; also see Fig. 6A). Subsequently, *col10a1* osteoblast progenitors were found to aggregate at lesion sites and differentiated into *osx*-positive mature osteoblasts, facilitating *de novo* mineralization (Renn et al., 2013; also see Fig. 6A, red arrows). At the same time, *col10a1* osteoblast progenitors lining the neural arches vanished (Renn et al., 2013; also see Fig. 6A, white arrows), raising the possibility that these cells could migrate to the lesion sites in vertebral bodies in order to repair bone. Time-lapse imaging over a 12 h period using the *col10a1*:GFP transgenic line showed that in the absence of Rankl induction, *col10a1*:GFP cells located at the tip of the neural arch exclusively migrated dorsally (Fig. S8A, red arrows; *n*=5 fish; Movie 1). In contrast, after Rankl induction, a subset of *col10a1*:GFP cells at the tip of the neural arch switched migration direction and moved ventrally towards the vertebral centra (Fig. S8B, yellow arrows; *n*=5 fish). However, 12 h time-lapse videos were unable to detect migration of *col10a1* cells all the way from the neural arches to the vertebral centra. Displacement tracks generated from time-lapse videos showed that in a 12 h period, *col10a1* cells were displaced less than 10 µm from their original position (Fig. S8A,B).

Thus, to trace the fate of *col10a1* osteoblast progenitors at neural arches after Rankl induction over a longer time period, we crossed *col10a1*$^{p2a\text{-}CreERT2}$|GaudiBBW2.1 fish with *rankl*:HSE:CFP fish (Fig. 6B). Embryos heterozygous for *col10a1*$^{p2a\text{-}CreERT2}$, GaudiBBW2.1 and *rankl*:HSE:CFP were treated with 4-HT at 7 dpf for *col10a1* cell labeling and heat-shocked at 9 dpf for Rankl induction (Fig. 6C). At 11 dpf, live confocal imaging was performed for a selection of larvae with labeled cells at the neural

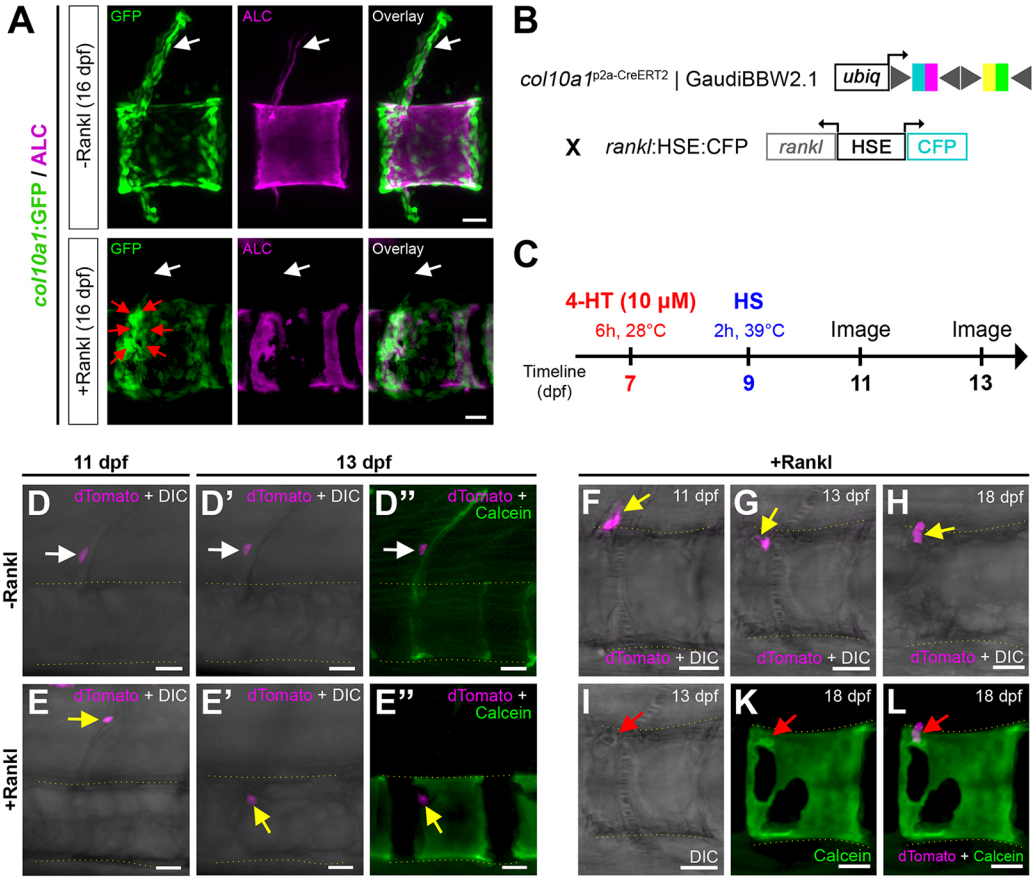

Fig. 6. Recruitment of *col10a1* osteoblast progenitors to bone lesion sites after Rankl induction. (A) *col10a1*:GFP expression and Alizarin complexone (ALC)-stained mineralized matrix in the vertebral column of *rankl*:HSE:*cfp*|*col10a1*:GFP medaka in the presence and absence of Rankl induction. Rankl was induced via a heat-shock at 9 dpf. (B,C) Strategy for tracking *col10a1* osteoblast progenitors after induction of bone lesions. Fish expressing the *col10a1*$^{p2a\text{-}CreERT2}$ Cre driver, Gaudi$^{BBW2.1}$ *loxP* reporter and *rankl*:HSE:*cfp* were used. At 7 dpf, fish were treated with 4-HT (10 µM; 6 h, 28°C) for Cre/*loxP* recombination-mediated cell labeling. At 9 dpf, fish were heat-shocked (39°C, 2 h) for Rankl induction. Live confocal imaging was performed at 11 and 13 dpf. (D-E″) Confocal images showing the location of dTomato-labeled cells at the vertebral column at 11 and 13 dpf. In the absence of Rankl induction, the neural arch labeled cell remained relatively immobile and did not migrate to the vertebral body (white arrows in D-D″; *n*=5/5 fish). After Rankl induction, the neural arch labeled cell migrated to the vertebral body where bone lesions had formed (yellow arrows in E-E″; *n*=5/7 fish). (F-L) Confocal images showing the migration and morphological changes of a dTomato-labeled cell (yellow arrows in F-H) from 11 to 18 dpf in a Rankl-induced medaka vertebral column. Red arrows in I-L indicate bone lesion sites that re-mineralized. Calcein was used for live staining of the mineralized bone matrix. Yellow dotted lines in D-L indicate the region where vertebral bodies are located. Scale bars: 25 µm.

Development (2022) 149, dev200238. doi:10.1242/dev.200238

arch. Out of 44 4-HT-treated larvae, 26 larvae (59.1%) had labeled cells in the vertebral column. Twelve larvae (27.3%) had a single labeled cell at a neural arch (Fig. 6D,E, arrows) and were raised until 13 dpf for imaging (Fig. 6D′,D″,E′,E″). In all 12 larvae, there was no increase in the number of labeled cells in the vertebral column from 11 to 13 dpf, indicating that *de novo* cell labeling did not occur and that labeled cells did not proliferate.

In the absence of Rankl induction, labeled cells at the neural arches remained at roughly the same position from 11 to 13 dpf and never migrated ventrally to the vertebral centra (Fig. 6D-D″, white arrows; *n*=5/5 fish). This is consistent with observations from time-lapse imaging of transgenic *col10a1*:GFP larvae at 11 dpf (Movie 1; Fig. S8A, red arrows; *n*=5 fish). In stark contrast, after Rankl induction, labeled cells that were previously at the neural arch were observed at the vertebral centra where mineralized matrix was degraded (Fig. 6E-E″, yellow arrows; *n*=5/7 fish). In addition, dynamic changes in the morphology of labeled cells were observed (Fig. 6F-H). Cell protrusions formed (Fig. 6G, yellow arrow) and retracted (Fig. 6H, yellow arrow) as labeled cells migrated to lesion sites where re-mineralization occurred (Fig. 6I-L, red arrows). These observations indicate that *col10a1* osteoblast progenitors residing at neural arches serve as an activatable source that can be triggered to facilitate bone repair upon formation of bone lesions in the medaka vertebral column.

DISCUSSION

The Cre/*loxP* recombination system has been widely used for genetic cell lineage tracing and fate-mapping studies in teleosts and mammals (Centanin et al., 2014; Harris et al., 2014; Kretzschmar and Watt, 2012; Tu and Johnson, 2011). For precise tracking of cell fate and lineages, it is crucial that Cre/*loxP* recombination is induced only in the specific cell type of interest. The use of transgenic Cre drivers with ectopic Cre expression may confound data interpretation and lead to false conclusions (Chakraborty et al., 2019; Song and Palmiter, 2018). In this study, we used CRISPR/Cas9 to generate *col10a1*$^{p2a\text{-}CreERT2}$ knock-in medaka where *CreERT2* expression is driven by the endogenous *col10a1* promoter. We show that knock-in fish developed bone and cartilage normally and survived without overt defects up to adulthood. In addition, *CreERT2* was expressed in a pattern identical to *col10a1* and could be induced by 4-HT for specific Cre/*loxP* recombination-labeling of *col10a1* cells. Using *col10a1*$^{p2a\text{-}CreERT2}$, we identified *col10a1* osteoblast progenitors at neural arches as a resident cellular source for recruited osteoblasts to repair osteoporotic bone lesions in the vertebral column. This highlights *col10a1*$^{p2a\text{-}CreERT2}$ as a useful tool for *col10a1* cell fate and lineage analyses during bone remodeling and repair in a vertebrate model suitable for live imaging.

Generation of a medaka *col10a1* Cre driver via a non-disruptive CRISPR/Cas9-mediated homology-directed repair approach

Tol2 transposon and I-SceI meganuclease are commonly used tools for the generation of transgenic Cre driver lines in zebrafish and medaka (Carney and Mosimann, 2018; Centanin et al., 2014). However, these transgenesis approaches make use of random integration of transgenes into the genome, often resulting in position effects. Depending on the regulatory environment at the location of transgene integration, transgene expression may be ectopically enhanced or silenced (Kondrychyn et al., 2009; Thermes et al., 2002). To overcome position effects, the CRISPR/Cas9 system has been used for targeted knock-in of transgenes (Kimura et al., 2014; Watakabe et al., 2018). In CRISPR/Cas9 knock-in approaches, DNA sequences are inserted into specific gene loci via non-homologous end joining (NHEJ) or homology-directed repair (HDR). Although NHEJ is more efficient compared with HDR, it is error-prone, and indels are often observed at knock-in sites (Albadri et al., 2017). On the other hand, HDR allows precise knock-in but has limited efficiency (Liu et al., 2019).

Two recent zebrafish studies have reported the generation of Cre driver lines via CRISPR/Cas9-mediated knock-in (Almeida et al., 2021; Kesavan et al., 2018). However, these approaches disrupted either the coding sequence or the expression level of target genes. Kesavan et al. inserted CreERT2 upstream of the endogenous start codon via NHEJ and they observed a reduction in expression of the target gene in knock-in fish. Almeida et al. knocked in CreERT2 at a coding exon via HDR, causing a loss-of-function mutation upon successful knock-in. Hence, the application of these approaches is limited for genes where knockdown or haploinsufficiency leads to a phenotype.

In comparison, our knock-in approach resulted in minimal interruption to the gene of interest. By targeting knock-in at the 3′ end of *col10a1*, we avoided disruption of regulatory elements near its transcription initiation site. In addition, making use of HDR for precise integration of the donor template, we inserted p2a-CreERT2 immediately before the stop codon of *col10a1*, preserving its coding sequence. Although bases at the *col10a1* gRNA site were edited to avoid CRISPR/Cas9 cleavage at the donor template 5′ homology arm, these modifications were silent as the protein-coding sequence of *col10a1* remained unchanged in knock-in fish. As the efficiency of HDR has been reported to be low (Liu et al., 2019), we included a *cmlc2*:EGFP secondary fluorescence reporter to accelerate the screening process. We observed high germline transmission rates when screening via *cmlc2*:EGFP expression (3/7, 42.9%). In addition, we found that *cmlc2*:EGFP expression was a good indicator of precise knock-in at the *col10a1* locus (2/3, 66.7%). With our screening strategy, the germline transmission rate of precise knock-in was 28.6% (2/7). This is markedly higher than the rate of 3% reported in Kesavan et al. (2018) and comparable with rates of 5% to 33% reported by Almeida et al. (2021). Using our knock-in strategy, we also successfully knocked in p2a-CreERT2 into the endogenous *osr1* and *col2a1a* loci, with similar knock-in efficiencies to *col10a1* at the F0 generation. Our approach therefore provides an efficient and non-disruptive method for generating knock-in Cre driver lines in medaka and zebrafish.

col10a1$^{p2a\text{-}CreERT2}$ as a useful tool for osteoblast progenitor labeling and fate tracing

For effective use of the Cre/Lox system to trace cell fate and lineages, it is important that cells are labeled in a specific and efficient manner. We previously generated transgenic *col10a1*:CreERT2-p2a-mCherry medaka for lineage tracing of *col10a1* cells in the regenerating adult fin (Dasyani et al., 2019). *col10a1*:CreERT2-p2a-mCherry expression matched endogenous *col10a1* expression in adult fin joint cells and osteoblasts, and could be induced to label *col10a1* cells with an efficiency of 61.5% (Dasyani et al., 2019; data not shown). However, compared with endogenous *col10a1*, expression of the transgene in the cranial skeleton and vertebral column was delayed during early development (data not shown). In addition, ectopic transgene expression was observed in spinal cord neurons (Fig. S4). Hence, the *col10a1*:CreERT2-p2a-mCherry transgenic line was not suitable for *col10a1* cell fate and lineage analyses in these structures. Here, we found that *CreERT2* RNA and protein expression in *col10a1*$^{p2a\text{-}CreERT2}$ medaka precisely recapitulated endogenous *col10a1*

Development (2022) 149, dev200238. doi:10.1242/dev.200238

expression in bone and cartilage structures at early developmental time points. In addition, similar to *col10a1*:CreERT2-p2a-mCherry, *col10a1*$^{p2a\text{-}CreERT2}$ is functional for Cre/*loxP* recombination-mediated cell labeling and lineage tracing of *col10a1* joint cells and osteoblasts in the adult fin. In heterozygous *col10a1*$^{p2a\text{-}CreERT2}$ medaka larvae, cell labeling efficiencies were 59.6% (34/57 fish) and 100% (20/20 fish) for 4-HT treatment durations of 6 h and 24 h, respectively. Hence, depending on the objectives of future studies, the treatment duration and concentration of 4-HT can be adjusted to control the extent of cell labeling. In addition, to further enhance cell labeling efficiency, homozygous *col10a1*$^{p2a\text{-}CreERT2}$ can be used. The *col10a1*$^{p2a\text{-}CreERT2}$ medaka line therefore serves as a versatile tool that can be used to accurately label *col10a1* cells for cell fate and lineage analyses in medaka.

Resident *col10a1* osteoblast progenitors at neural arches are recruited for bone lesion repair in the medaka vertebral column

For bone growth, homeostasis and repair, timely recruitment of osteoblasts and their progenitors to sites of bone deposition is crucial. Previous studies have shown that cellular sources of recruited osteoblasts include mesenchymal stem cells (Méndez-Ferrer et al., 2010; Park et al., 2012), periosteal osteoblast progenitors (Kegelman et al., 2021; Maes et al., 2010), pericytes (Crisan et al., 2008; Kalajzic et al., 2008) and hypertrophic chondrocytes (Giovannone et al., 2019; Yang et al., 2014; Zhou et al., 2014). However, molecular factors driving the migration of these cells to bone remodeling or repair sites remain poorly understood (Thiel et al., 2018). *In vitro* studies have identified chemoattractants [such as CXC motif chemokine ligand 16 (CXCL16; Ota et al., 2013)], bone morphogenetic protein 7 (BMP7; Lee et al., 2006), clastokines [such as the slit guidance ligand 3 (SLIT3; Kim et al., 2018)] and platelet-derived growth factors (PDGFs; Colciago et al., 2009) as stimulants of osteoblast migration. However, whether these molecules play a role in the recruitment of osteoblasts *in vivo* remains to be shown.

We have previously shown that *col10a1*:GFP osteoblast progenitors accumulate at Rankl-induced bone lesion sites and facilitate bone re-mineralization in the medaka vertebral column (Renn et al., 2013). However, the origin of these recruited osteoblast progenitors and the mechanism guiding their recruitment remain unclear. Owing to the limitations of live time-lapse imaging, i.e. photobleaching of fluorophores and reduced survival of larvae after 12 h of imaging, recruitment of *col10a1* osteoblast progenitors from neural arches to bone lesion sites could not be detected using the *col10a1*:GFP transgenic line. Here, by using the *col10a1*$^{p2a\text{-}CreERT2}$ knock-in line to track *col10a1* cells over 48 h, we found that *col10a1* osteoblast progenitors residing at neural arches can be triggered to migrate to bone lesion sites at vertebral centra for bone repair. Without Rankl induction, migration of *col10a1* osteoblast progenitors from neural arches to vertebral centra was never observed and these cells appeared stationary. Hence, we speculate that, upon formation of Rankl-induced bone lesions, specific chemotactic factors are released from the lesion sites. Chemotactic gradients then activate migratory behavior of *col10a1* osteoblast progenitors, which form cell projections and move towards the chemical cues. Future analysis on cell-surface receptors and molecular networks activated in these recruited *col10a1* cells will provide valuable insights into the mechanisms driving osteoblast recruitment. Our medaka model also serves as a useful *in vivo* platform for the study of molecules previously proposed to regulate osteoblast migration *in vitro*. Such studies would greatly facilitate the development of bone anabolic therapies for treatment of low bone mass disorders such as osteoporosis, as well as for the stimulation of bone fracture repair.

MATERIALS AND METHODS

Maintenance of medaka lines

Medaka lines were maintained under a controlled 14 h light/10 h dark cycle in the fish facilities at the National University of Singapore. Fish breeding and experiments were performed in accordance with protocols approved by the Institutional Animal Care and Use Committee of the National University of Singapore (protocol numbers BR19-0120 and R18-0562). The medaka Cab strain was used as wild type. Transgenic *col10a1*:GFP (Renn et al., 2013), *rankl*:HSE:CFP (To et al., 2012), GaudiRSG and GaudiBBW2.1 (Centanin et al., 2014) lines have been previously described.

Generation of *col10a1*, *osr1* and *col2a1a* knock-in donor plasmids

For cloning of the knock-in donor plasmids, 5′ and 3′ *col10a1*, *osr1* and *col2a1a* homology arms were PCR amplified from genomic DNA of wild-type medaka. p2a-CreERT2-pA was PCR amplified from plasmid *col10a1*:CreERT2-p2a-mCherry (Dasyani et al., 2019) and *cmlc2*:EGFP-pA was PCR amplified from plasmid pBS/I-*Sce*I/*Hsp70*::Cre-NLS (kindly provided by Lazaro Centanin, Centre for Organismal Studies, Heidelberg, Germany; Centanin et al., 2014). All PCR primers used are listed in Table S1. The mbait guide RNA (gRNA) sequence used has been described previously (Kimura et al., 2014) and is listed in Table S2. *col10a1*, *osr1* and *col2a1a* gRNA target sequences were selected using the CCTop web tool (Stemmer et al., 2015; Table S2). Wobble bases at the *col10a1*, *osr1* and *col2a1a* gRNA sites in the respective donor plasmids were introduced by PCR using primers with mismatched nucleotides (Table S1). The homology arms, mbait, p2a-CreERT2-pA and *cmlc2*:EGFP-pA sequences were combined in the order as shown in Fig. 1, Figs S2A and S3A for *col10a1*, *osr1* and *col2a1a*, respectively, by PCR using overlapping primers (Table S1). For the *col10a1* donor plasmid, the mbait-5′HA-p2a-CreERT2-pA-*cmlc2*:EGFP-pA-3′HA-mbait insert was ligated to a pCR-bluntII-TOPO vector (Invitrogen). For *osr1* and *col2a1a* donor plasmids, the mbait-5′HA-p2a-CreERT2-pA-*cmlc2*:EGFP-pA-3′HA-mbait insert were ligated to a pJET1.2/blunt vector (ThermoFisher Scientific). All donor plasmids can be obtained from Addgene (Addgene 184874, 184875 and 184876 for *col10a1*, *osr1* and *col2a1a*, respectively).

Establishment of *col10a1*$^{p2a\text{-}CreERT2}$, *osr1*$^{p2a\text{-}CreERT2}$ and *col2a1a*$^{p2a\text{-}CreERT2}$ medaka

A solution containing the donor plasmid (20 ng/µl), Cas9 protein (0.25 µg/µl; Integrated DNA Technologies, IDT), mbait crRNA (36 ng/µl; IDT), tracrRNA (67 ng/µl; IDT) and the respective *col10a1*, *osr1* or *col2a1a* crRNA (36 ng/µl; IDT) was injected into wild-type medaka embryos at the one-cell stage. Injected embryos were screened for *cmlc2*:EGFP expression at 12 days post-fertilization (dpf). To establish a stable *col10a1*$^{p2a\text{-}CreERT2}$ line, *cmlc2*:EGFP-positive larvae were raised to adulthood and out-crossed to wild-type medaka. F1 offspring positive for *cmlc2*:EGFP expression were raised and subsequently fin clipped for PCR genotyping to determine whether knock-in occurred at the endogenous *col10a1* locus (primers listed in Table S1). DNA sequencing was performed to confirm precise integration of the donor template at the 3′ and 5′ *col10a1* homology regions (primers listed in Table S1). Primers used for genotyping of heterozygous and homozygous *col10a1*$^{p2a\text{-}CreERT2}$ knock-in fish are listed in Table S1. To confirm precise knock-in of the donor template in *osr1*$^{p2a\text{-}CreERT2}$ and *col2a1a*$^{p2a\text{-}CreERT2}$ potential founders (F0), 12 dpf *cmlc2*:EGFP-positive larvae were fin clipped for PCR genotyping, and DNA sequencing was performed (primers listed in Table S1).

Riboprobe generation, *in situ* hybridization and immunohistochemistry

The *col10a1* riboprobe was generated as previously reported (Renn and Winkler, 2010). To generate the *CreERT2* riboprobe, a 637 bp *CreERT2*

sequence was amplified from the knock-in donor plasmid using primers CreERT2_366_FP (5′-GAAAACGTTGATGCCGGTGAAC-3′) and CreERT2_1003_RP (5′-TTGCCCCTGTTTCACTATCCAGG-3′). This sequence was then ligated to a pCR-bluntII-TOPO vector (Invitrogen) containing flanking T7 and SP6 promoter sequences. To synthesize *CreERT2* sense and antisense riboprobes, plasmid linearization was performed using the respective SpeI and XbaI restriction enzyme (New England Biolabs) and *in vitro* transcription was performed using T7 and SP6 RNA polymerase (DIG RNA Labeling Mix, Roche), respectively. Whole-mount RNA *in situ* hybridization was performed as described by Renn and Winkler (2009). Immunohistochemistry on medaka cryosections (20 µm) was performed as previously described (Dasyani et al., 2019). Mouse anti-Cre Recombinase antibody (1:400, Merck MAB3120, Clone 2D8, lot 3543072) and secondary goat anti-mouse Alexa Fluor 633 (1:500, Invitrogen A-21052) were used.

Bone and cartilage staining

Live bone staining using Alizarin complexone (ALC; Sigma A3882) or Calcein (Sigma C0875) was performed as described by Renn et al. (2013). For fixed samples, staining of bone using Alizarin Red S (Sigma A5533) and cartilage using Alcian Blue 8GX (Sigma A3157) were performed as described by Renn and Winkler, 2009.

4-hydroxytamoxifen treatment

To induce Cre/*loxP* recombination at embryonic stages (7 to 9 dpf), *col10a1*$^{p2a\text{-}CreERT2}$|GaudiRSG or *col10a1*$^{p2a\text{-}CreERT2}$|GaudiBBW2.1 embryos were incubated in 10 µM 4-hydroxytamoxifen (4-HT; Sigma T176) for 6 or 24 h in the dark at 28°C. After 4-HT treatment, fish were washed thrice with 1× fish medium [19.3 mM NaCl, 0.23 mM KCl, 0.13 mM $MgSO_4$, 0.2 mM $Ca(NO_3)_2$, and1.7 mM HEPES (pH 7.0)]. To induce Cre/*loxP* recombination in *col10a1*$^{p2a\text{-}CreERT2}$|GaudiRSG adults (5 months old), fish were treated with 0.5 µM 4-HT for 72 h in the dark. After 4-HT treatment, fish were washed thrice with fish system water.

Rankl induction and *col10a1* cell fate tracking

Embryos from a cross of *col10a1*$^{p2a\text{-}CreERT2}$|GaudiBBW2.1 and *rankl*:HSE:CFP were used. At 7 dpf, Cre/*loxP* recombination-mediated *col10a1* cell labeling was performed via 4-HT treatment (10 µM, 6 h, 28°C). At 9 dpf, Rankl induction was conducted via a heat-shock at 39°C for 2 h. After heat-shock, embryos were kept in a 30°C incubator and live confocal imaging was performed at 11 and 13 dpf.

Fin regeneration analysis

Amputation of the adult medaka fin and imaging of the regenerating fin were performed as described by Dasyani et al. (2019).

Quantification of cells

Quantification of *col10a1*:GFP cells was performed as described by Phan et al. (2020). To quantify nlsEGFP-labelled cells in *col10a1*$^{p2a\text{-}CreERT2}$|GaudiRSG medaka, cells were counted manually.

Imaging

Images were captured using the Olympus FluoView FV3000 confocal microscope, Zeiss LSM900 confocal microscope and Nikon SMZ18 stereomicroscope. For live fluorescence imaging, larvae were anaesthetized in 0.016% Tricaine (Sigma MS-222) and mounted in 1.2% low melting agarose on a glass-bottom dish. Image processing was performed using Fiji ImageJ, Bitplane Imaris and Adobe Photoshop.

Acknowledgements

We thank Lazaro Centanin (Centre for Organismal Studies, University of Heidelberg) for sharing the pBS/I-*Sce*I/*Hsp70*::Cre-NLS plasmid as well as the GaudiRSG and GaudiBBW2.1 transgenic lines. We also thank the Centre for Bioimaging Sciences (CBIS) confocal unit and the fish facility at Department of Biological Sciences, National University of Singapore for continued support.

Competing interests

The authors declare no competing or financial interests.

Author contributions

Conceptualization: W.H.T., C.W.; Methodology: W.H.T.; Formal analysis: W.H.T.; Investigation: W.H.T.; Writing - original draft: W.H.T., C.W.; Writing - review & editing: C.W.; Supervision: C.W.; Funding acquisition: C.W.

Funding

This work was supported by the Ministry of Education – Singapore (MOE2016-T2-2-086, MOE2016-T3-1-005 and AcRF R-154-000-C78-114) and the National Research Foundation Singapore (NRF2017-NRF-ISF002-2671).

Peer review history

The peer review history is available online at https://journals.biologists.com/dev/article-lookup/doi/10.1242/dev.200238

References

Albadri, S., Del Bene, F. and Revenu, C. (2017). Genome editing using CRISPR/Cas9-based knock-in approaches in zebrafish. *Methods* **121-122**, 77-85. doi:10.1016/j.ymeth.2017.03.005

Almeida, M. P., Welker, J. M., Siddiqui, S., Luiken, J., Ekker, S. C., Clark, K. J., Essner, J. J. and McGrail, M. (2021). Endogenous zebrafish proneural Cre drivers generated by CRISPR/Cas9 short homology directed targeted integration. *Sci. Rep.* **11**, 1732. doi:10.1038/s41598-021-81239-y

Bragdon, B. C. and Bahney, C. S. (2018). Origin of reparative stem cells in fracture healing. *Curr. Osteoporos Rep.* **16**, 490-503. doi:10.1007/s11914-018-0458-4

Carney, T. J. and Mosimann, C. (2018). Switch and trace: recombinase genetics in Zebrafish. *Trends Genet.* **34**, 362-378. doi:10.1016/j.tig.2018.01.004

Centanin, L., Ander, J.-J., Hoeckendorf, B., Lust, K., Kellner, T., Kraemer, I., Urbany, C., Hasel, E., Harris, W. A., Simons, B. D. et al. (2014). Exclusive multipotency and preferential asymmetric divisions in post-embryonic neural stem cells of the fish retina. *Development (Cambridge, England)* **141**, 3472-3482. doi:10.1242/dev.109892

Chakraborty, R., Saddouk, F. Z., Carrao, A. C., Krause, D. S., Greif, D. M. and Martin, K. A. (2019). Promoters to study vascular smooth muscle. *Arterioscler. Thromb. Vasc. Biol.* **39**, 603-612. doi:10.1161/ATVBAHA.119.312449

Colciago, A., Celotti, F., Casati, L., Giancola, R., Castano, S. M., Antonini, G., Sacchi, M. C. and Negri-Cesi, P. (2009). In Vitro effects of PDGF isoforms (AA, BB, AB and CC) on migration and proliferation of SaOS-2 osteoblasts and on migration of human osteoblasts. *Int. J. Biomed. Sci.* **5**, 380-389.

Crisan, M., Yap, S., Casteilla, L., Chen, C.-W., Corselli, M., Park, T. S., Andriolo, G., Sun, B., Zheng, B., Zhang, L. et al. (2008). A perivascular origin for mesenchymal stem cells in multiple human organs. *Cell Stem Cell* **3**, 301-313. doi:10.1016/j.stem.2008.07.003

Dasyani, M., Tan, W. H., Sundaram, S., Imangali, N., Centanin, L., Wittbrodt, J. and Winkler, C. (2019). Lineage tracing of col10a1 cells identifies distinct progenitor populations for osteoblasts and joint cells in the regenerating fin of medaka (Oryzias latipes). *Dev. Biol.* **455**, 85-99. doi:10.1016/j.ydbio.2019.07.012

Dirckx, N., Van Hul, M. and Maes, C. (2013). Osteoblast recruitment to sites of bone formation in skeletal development, homeostasis, and regeneration. *Birth Defects Research Part C: Embryo Today: Reviews* **99**, 170-191. doi:10.1002/bdrc.21047

Donnelly, M. L. L., Hughes, L. E., Luke, G., Mendoza, H., ten Dam, E., Gani, D. and Ryan, M. D. (2001). The 'cleavage' activities of foot-and-mouth disease virus 2A site-directed mutants and naturally occurring '2A-like' sequences. *J. Gen. Virol.* **82**, 1027-1041. doi:10.1099/0022-1317-82-5-1027

Eames, B. F., Amores, A., Yan, Y. L. and Postlethwait, J. H. (2012). Evolution of the osteoblast: skeletogenesis in gar and zebrafish. *BMC Evol. Biol.* **12**, 27. doi:10.1186/1471-2148-12-27

Einhorn, T. A. and Gerstenfeld, L. C. (2015). Fracture healing: mechanisms and interventions. *Nat. Rev. Rheumatol.* **11**, 45-54. doi:10.1038/nrrheum.2014.164

Fu, X., Liu, Q., Li, C., Li, Y. and Wang, L. (2020). Cardiac fibrosis and cardiac fibroblast lineage-tracing: recent advances. *Front. Physiol.* **11**, 416. doi:10.3389/fphys.2020.00416

Geurtzen, K., Knopf, F., Wehner, D., Huitema, L. F., Schulte-Merker, S. and Weidinger, G. (2014). Mature osteoblasts dedifferentiate in response to traumatic bone injury in the zebrafish fin and skull. *Development* **141**, 2225-2234. doi:10.1242/dev.105817

Giovannone, D., Paul, S., Schindler, S., Arata, C., Farmer, D. T., Patel, P., Smeeton, J. and Crump, J. G. (2019). Programmed conversion of hypertrophic chondrocytes into osteoblasts and marrow adipocytes within zebrafish bones. *Elife* **8**, e42736. doi:10.7554/eLife.42736

Hadjidakis, D. J. and Androulakis, I. I. (2006). Bone remodeling. *Ann N Y Acad Sci,* **1092**, 385-396. doi:10.1196/annals.1365.035

Harris, J. A., Hirokawa, K. E., Sorensen, S. A., Gu, H., Mills, M., Ng, L. L., Bohn, P., Mortrud, M., Ouellette, B. and Kidney, J. (2014). Anatomical characterization of Cre driver mice for neural circuit mapping and manipulation. *Front. Neural Circuits* **8**, 76. doi:10.3389/fncir.2014.00076

Hengartner, N.-E., Fiedler, J., Ignatius, A. and Brenner, R. E. (2013). IL-1β inhibits human osteoblast migration. *Mol. Med.* **19**, 36-42. doi:10.2119/molmed.2012.00058
Hu, D. P., Ferro, F., Yang, F., Taylor, A. J., Chang, W., Miclau, T., Marcucio, R. S. and Bahney, C. S. (2017). Cartilage to bone transformation during fracture healing is coordinated by the invading vasculature and induction of the core pluripotency genes. *Development* **144**, 221-234. doi:10.1242/dev.130807
Kalajzic, Z., Li, H., Wang, L. P., Jiang, X., Lamothe, K., Adams, D. J., Aguila, H. L., Rowe, D. W. and Kalajzic, I. (2008). Use of an alpha-smooth muscle actin GFP reporter to identify an osteoprogenitor population. *Bone* **43**, 501-510. doi:10.1016/j.bone.2008.04.023
Kegelman, C. D., Nijsure, M. P., Moharrer, Y., Pearson, H. B., Dawahare, J. H., Jordan, K. M., Qin, L. and Boerckel, J. D. (2021). YAP and TAZ promote periosteal osteoblast precursor expansion and differentiation for fracture repair. *J. Bone Miner. Res.* **36**, 143-157. doi:10.1002/jbmr.4166
Kesavan, G., Hammer, J., Hans, S. and Brand, M. (2018). Targeted knock-in of CreER (T2) in zebrafish using CRISPR/Cas9. *Cell Tissue Res.* **372**, 41-50. doi:10.1007/s00441-018-2798-x
Kim, B. J., Lee, Y. S., Lee, S. Y., Baek, W. Y., Choi, Y. J., Moon, S. A., Moon, S. A., Lee, S. H., Kim, J.-E., Chang, E.-J. et al. (2018). Osteoclast-secreted SLIT3 coordinates bone resorption and formation. *J. Clin. Invest.* **128**, 1429-1441. doi:10.1172/JCI91086
Kimura, Y., Hisano, Y., Kawahara, A. and Higashijima, S.-i. (2014). Efficient generation of knock-in transgenic zebrafish carrying reporter/driver genes by CRISPR/Cas9-mediated genome engineering. *Sci. Rep.* **4**, 6545. doi:10.1038/srep06545
Knopf, F., Hammond, C., Chekuru, A., Kurth, T., Hans, S., Weber, C. W., Mahatma, G., Fisher, S., Brand, M., Schulte-Merker, S. et al. (2011). Bone regenerates via dedifferentiation of osteoblasts in the zebrafish fin. *Dev. Cell* **20**, 713-724. doi:10.1016/j.devcel.2011.04.014
Kondrychyn, I., Garcia-Lecea, M., Emelyanov, A., Parinov, S. and Korzh, V. (2009). Genome-wide analysis of Tol2 transposon reintegration in zebrafish. *BMC Genomics* **10**, 418. doi:10.1186/1471-2164-10-418
Kretzschmar, K. and Watt, F. M. (2012). Lineage tracing. *Cell* **148**, 33-45. doi:10.1016/j.cell.2012.01.002
Lee, D. H., Park, B. J., Lee, M.-S., Lee, J. W., Kim, J. K., Yang, H.-C. and Park, J.-C. (2006). Chemotactic migration of human mesenchymal stem cells and MC3T3-E1 osteoblast-like cells induced by COS-7 cell line expressing rhBMP-7. *Tissue Eng.* **12**, 1577-1586. doi:10.1089/ten.2006.12.1577
Lee, R. T. H., Asharani, P. V. and Carney, T. J. (2014). Basal keratinocytes contribute to all strata of the adult Zebrafish epidermis. *PLoS One* **9**, e84858. doi:10.1371/journal.pone.0084858
Liu, M., Rehman, S., Tang, X., Gu, K., Fan, Q., Chen, D. and Ma, W. (2019). Methodologies for improving HDR efficiency. *Front. Genet.* **9**, 691. doi:10.3389/fgene.2018.00691
Livet, J., Weissman, T. A., Kang, H., Draft, R. W., Lu, J., Bennis, R. A., Sanes, J. R. and Lichtman, J. W. (2007). Transgenic strategies for combinatorial expression of fluorescent proteins in the nervous system. *Nature* **450**, 56-62. doi:10.1038/nature06293
Lleras-Forero, L., Winkler, C. and Schulte-Merker, S. (2019). Zebrafish and medaka as models for biomedical research of bone diseases. *Dev. Biol.* **457**, 191-205. doi:10.1016/j.ydbio.2019.07.009
Maes, C., Kobayashi, T., Selig, M. K., Torrekens, S., Roth, S. I., Mackem, S., Carmeliet, G. and Kronenberg, H. M. (2010). Osteoblast precursors, but not mature osteoblasts, move into developing and fractured bones along with invading blood vessels. *Dev. Cell* **19**, 329-344. doi:10.1016/j.devcel.2010.07.010
Méndez-Ferrer, S., Michurina, T. V., Ferraro, F., Mazloom, A. R., Macarthur, B. D., Lira, S. A., Scadden, D. T., Ma'ayan, A. and Enikolopov, G. N. (2010). Mesenchymal and haematopoietic stem cells form a unique bone marrow niche. *Nature* **466**, 829-834. doi:10.1038/nature09262
Nakasaki, M., Yoshioka, K., Miyamoto, Y., Sasaki, T., Yoshikawa, H. and Itoh, K. (2008). IGF-I secreted by osteoblasts acts as a potent chemotactic factor for osteoblasts. *Bone* **43**, 869-879. doi:10.1016/j.bone.2008.07.241
Ota, K., Quint, P., Weivoda, M. M., Ruan, M., Pederson, L., Westendorf, J. J., Khosla, S. and Oursler, M. J. (2013). Transforming growth factor beta 1 induces CXCL16 and leukemia inhibitory factor expression in osteoclasts to modulate migration of osteoblast progenitors. *Bone* **57**, 68-75. doi:10.1016/j.bone.2013.07.023
Otsuru, S., Tamai, K., Yamazaki, T., Yoshikawa, H. and Kaneda, Y. (2008). Circulating bone marrow-derived osteoblast progenitor cells are recruited to the bone-forming site by the CXCR4/stromal cell-derived factor-1 pathway. *Stem Cells* **26**, 223-234. doi:10.1634/stemcells.2007-0515
Pan, Y. A., Freundlich, T., Weissman, T. A., Schoppik, D., Wang, X. C., Zimmerman, S., Ciruna, B., Sanes, J. R., Lichtman, J. W. and Schier, A. F. (2013). Zebrabow: multispectral cell labeling for cell tracing and lineage analysis in zebrafish. *Development* **140**, 2835-2846. doi:10.1242/dev.094631
Park, D., Spencer, J. A., Koh, B. I., Kobayashi, T., Fujisaki, J., Clemens, T. L., Lin, C. P., Kronenberg, H. M. and Scadden, D. T. (2012). Endogenous bone marrow MSCs are dynamic, fate-restricted participants in bone maintenance and regeneration. *Cell Stem Cell* **10**, 259-272. doi:10.1016/j.stem.2012.02.003
Phan, Q. T., Tan, W. H., Liu, R., Sundaram, S., Buettner, A., Kneitz, S., Cheong, B., Vyas, H., Mathavan, S., Schartl, M. et al. (2020). Cxcl9l and Cxcr3.2 regulate recruitment of osteoclast progenitors to bone matrix in a medaka osteoporosis model. *Proc. Natl. Acad. Sci. USA* **117**, 19276-19286. doi:10.1073/pnas.2006093117
Renn, J. and Winkler, C. (2009). Osterix-mCherry transgenic medaka for in vivo imaging of bone formation. *Dev. Dyn.* **238**, 241-248. doi:10.1002/dvdy.21836
Renn, J. and Winkler, C. (2010). Characterization of collagen type 10a1 and osteocalcin in early and mature osteoblasts during skeleton formation in medaka. *J. Appl. Ichthyol.* **26**, 196-201. doi:10.1111/j.1439-0426.2010.01404.x
Renn, J. and Winkler, C. (2012). Osterix:nlGFP transgenic medaka identify regulatory roles for retinoic acid signaling during osteoblast differentiation in vivo. *J. Appl. Ichthyol.* **28**, 360-363. doi:10.1111/j.1439-0426.2012.01983.x
Renn, J., Buttner, A., To, T. T., Chan, S. J. and Winkler, C. (2013). A col10a1:nlGFP transgenic line displays putative osteoblast precursors at the medaka notochordal sheath prior to mineralization. *Dev. Biol.* **381**, 134-143. doi:10.1016/j.ydbio.2013.05.030
Rosa, J. T., Laizé, V., Gavaia, P. J. and Cancela, M. L. (2021). Fish models of induced osteoporosis. *Front. Cell Dev. Biol.* **9**, 1294. doi:10.3389/fcell.2021.672424
Shen, G. (2005). The role of type X collagen in facilitating and regulating endochondral ossification of articular cartilage. *Orthod. Craniofac. Res.* **8**, 11-17. doi:10.1111/j.1601-6343.2004.00308.x
Song, A. J. and Palmiter, R. D. (2018). Detecting and avoiding problems when using the Cre-lox system. *Trends Genet.* **34**, 333-340. doi:10.1016/j.tig.2017.12.008
Stemmer, M., Thumberger, T., Del Sol Keyer, M., Wittbrodt, J. and Mateo, J. L. (2015). CCTop: an intuitive, flexible and reliable CRISPR/Cas9 target prediction tool. *PLoS One* **10**, e0124633. doi:10.1371/journal.pone.0124633
Thermes, V., Grabher, C., Ristoratore, F., Bourrat, F., Choulika, A., Wittbrodt, J. and Joly, J.-S. (2002). I-SceI meganuclease mediates highly efficient transgenesis in fish. *Mech. Dev.* **118**, 91-98. doi:10.1016/S0925-4773(02)00218-6
Thiel, A., Reumann, M. K., Boskey, A., Wischmann, J., von Eisenhart-Rothe, R. and Mayer-Kuckuk, P. (2018). Osteoblast migration in vertebrate bone. *Biol. Rev. Camb. Philos. Soc.* **93**, 350-363. doi:10.1111/brv.12345
To, T. T., Witten, P. E., Renn, J., Bhattacharya, D., Huysseune, A. and Winkler, C. (2012). Rankl-induced osteoclastogenesis leads to loss of mineralization in a medaka osteoporosis model. *Development* **139**, 141-150. doi:10.1242/dev.071035
Tonelli, F., Bek, J. W., Besio, R., De Clercq, A., Leoni, L., Salmon, P., Coucke, P. J., Willaert, A. and Forlino, A. (2020). Zebrafish: a resourceful vertebrate model to investigate skeletal disorders. *Front. Endocrinol.* **11**, 489. doi:10.3389/fendo.2020.00489
Tu, S. and Johnson, S. L. (2011). Fate restriction in the growing and regenerating zebrafish fin. *Dev. Cell* **20**, 725-732. doi:10.1016/j.devcel.2011.04.013
Valenti, M. T., Marchetto, G., Mottes, M. and Dalle Carbonare, L. (2020). Zebrafish: a suitable tool for the study of cell signaling in bone. *Cells* **9**, 1911. doi:10.3390/cells9081911
Watakabe, I., Hashimoto, H., Kimura, Y., Yokoi, S., Naruse, K. and Higashijima, S. I. (2018). Highly efficient generation of knock-in transgenic medaka by CRISPR/Cas9-mediated genome engineering. *Zool. Lett.* **4**, 3. doi:10.1186/s40851-017-0086-3
Witten, P. E., Harris, M. P., Huysseune, A. and Winkler, C. (2017). Small teleost fish provide new insights into human skeletal diseases. *Method Cell Biol.* **138**, 321-346. doi:10.1016/bs.mcb.2016.09.001
Yang, L., Tsang, K. Y., Tang, H. C., Chan, D. and Cheah, K. S. (2014). Hypertrophic chondrocytes can become osteoblasts and osteocytes in endochondral bone formation. *Proc. Natl. Acad. Sci. USA* **111**, 12097-12102. doi:10.1073/pnas.1302703111
Zhou, X., von der Mark, K., Henry, S., Norton, W., Adams, H. and de Crombrugghe, B. (2014). Chondrocytes transdifferentiate into osteoblasts in endochondral bone during development, postnatal growth and fracture healing in mice. *PLoS Genet.* **10**, e1004820. doi:10.1371/journal.pgen.1004820

Table S1. List of primers.

Purpose	Primer	
	Name	Sequence (5' – 3')
Cloning of *col10a1* knock-in donor plasmid	Mbait9bp_FP	TTACGCCAGTCGACCACCTCTG
	Cre_pA_RP	CCCCACTTTGTACAAGATCAAGCTGTGGCAGGG AAAC
	Cre_pA_FP	TCCCTGCCACAGCTTGATCTTGTACAAAGTGGGGGAT
	Cmlc_HA2_RP	GATGCGTGATCAACCTAAAAGCTTAAATCAGTTGTGT
	Cmlc_HA2_FP	CAACTGATTTAAGCTTTTAGGTTGATCACGCATCAGG
	Mbait2bp_RP	AGCGCGCAATTAACCCTCACTCC
	P2A_Cre_FP1	CCCTGGACCTATGTCCAATTTACTAACCGTACACCA
	stopHA2_Cre_RP1	GTGATCAACCTATCAAGCTGTGGCAGGGAAACCCTCT
	P2a_HA1_RP1	AGTTTGTAGCCGTTGAAGCGATGAGAAAACCG
	Cre_stop_HA2_FP1	GCCACAGCTTGATAGGTTGATCACGCATCAGGTTC
	HA1_p2a_FP1	CTCATCGCTTCAACGGCTACAAACTTCAGCCTGCTG
	Mbait_cre_FP	CCCCCCCACCTCTGGAACCGCAGCAGCCATGTC CAATTTACTAACCGTA
	PolyA_mbait_RP	CCCCCCCACCTCTGGAACCGCAGCAGCCAAAA AACCTCCCACACCTCC
	HR_cre_mbait_RP	GTGGCGTCGACTGTATCTCCCTATGGGGTGAAA CAGCAGA
	HR_polyA_mbait_FP	GTGTGGGAGGTTTTTTGGTGGGAGCACTTTTTT GCCGTTCC
Cloning of *col2a1a* knock-in donor plasmid	c2o1_mbait_FP1	TTACGCCAGTCGACCACCTC
	mbait_c2HA1_RP1	GGTTTCCTGTGGCCGGGCTATGGGGTGAAACAGC
	mbait_c2HA1_FP1	GTTTCACCCCATAGCCCGGCCACAGGAAACCTGAAGA
	c2HA1_p2a_RP1	GGCTGAAGTTTGTAGCCAAAAAGCAGACGGGGCCTATGT
	c2HA1_p2a_FP1	GCCCCGTCTGCTTTTTGGCTACAAACTTCAGCCTGCTGA
	cmlc2_c2HA2_RP1	GTTGCAATACTCAACTAAAGCTTAAATCAGTTGTGTT
	cmlc2_c2HA2_FP1	AACTGATTTAAGCTTTAGTTGAGTATTGCAACGGCCC
	c2HA2_mbait_RP1	ACGGCAAAAAAGTGCTCTATTGCCGGTGCCCTTAAGT
	c2HA2_mbait_FP1	AGGGCACCGGCAATAGAGCACTTTTTTGCCGTTCC
	c2o1_mbait_RP1	CAAGCTATGCATCAAGCTTGGTACCCTC
Cloning of *osr1* knock-in donor plasmid	c2o1_mbait_FP1	TTACGCCAGTCGACCACCTC
	mbait_o1HA1_RP1	AAAAATGGCTGAGGGCTATGGGGTGAAACAGC
	mbait_o1HA1_FP1	TTTCACCCCATAGCCCTCAGCCATTTTTAGCGG
	o1HA1_p2a_RP1	GCTGAAGTTTGTAGCCTTGACCTTGGCTGGCTT
	o1HA1_p2a_FP1	CCAGCCAAGGTCAAGGCTACAAACTTCAGCCT
	cmlc2_o1HA2_RP1	TGTCCCGGTCGCTTGACAAAGCTTAAATCAGTTGTG
	cmlc2_o1HA2_FP1	AACTGATTTAAGCTTTGTCAAGCGACCGGGACACT

	o1HA2_mbait_RP1	GGCAAAAAAGTGCTCCACAGGGGTTTTTCAAGGTCC
	o1HA2_mbait_FP1	CTTGAAAAACCCCTGTGGAGCACTTTTTTGCCGT
	c2o1_mbait_RP1	CAAGCTATGCATCAAGCTTGGTACCCTC
Incorporation of *col10a1* wobble bases	pA_Col10a1_e2wob_FP	GGGAGGTGTGGGAGGTTTTTTCTGCACTTTCTCTGGGTTC CTGATTGC
	Col10a1e2endwob_RP	AAAACCGGAAAACGTACAATGTACATTCTCAGCAGCAAA GACACCATTGG
Incorporation of *col2a1a* wobble bases	c2wob_FP1	AAAACCTCACGCTTGCCCATAGTCGAC
	c2wob_RP1	GTCGACTATGGGCAAGCGTGAGGTTTT
Incorporation of *osr1* wobble bases	o1wob_FP1	TTTGCTGCGATCAGCACAGGTGGGTCA
	o1wob_RP1	TGACCCACCTGTGCTGATCGCAGCAAA
Genotyping of *col10a1*$^{p2a\text{-}CreERT2}$ medaka	Col10a1_e2_1481_FP (FP1)	GGCAGCCCCATTAAGTTCGACC
	CreERT2_81_RP (RP1)	GGCGATCCCTGAACATGTCCAT
	Col10a1_i2_244_RP (RP2)	TGTCTCCGTTACAAAAGGTCACCG
Sequencing of *col10a1* knock-in at 3' and 5' homology regions	Col10a1_e2_1481_FP	GGCAGCCCCATTAAGTTCGAC
	CreERT2_81_RP	GGCGATCCCTGAACATGTCCAT
	Col10a1_i2_244_RP	TGTCTCCGTTACAAAAGGTCACCG
	GFP_66_RP	GTCGCCGTCCAGCTCGACCA
Sequencing of *col2a1a* knock-in at 3' and 5' homology regions	c2a1a_i53_FP (FP1)	AAGGGCCATCTTCTGAGTGGA
	CreERT2_81_RP (RP1)	GGCGATCCCTGAACATGTCCAT
	col2a1_end_RP1 (RP2)	AACTTGGTTTGCTTGGTCCCT
	GFP_66_RP (FP2)	GTCGCCGTCCAGCTCGACCA
Sequencing of *osr1* knock-in at 3' and 5' homology regions	osr1_i1_1296_FP (FP1)	TTGCACTGGAGAAGGGGTTTAG
	CreERT2_81_RP (RP1)	GGCGATCCCTGAACATGTCCAT
	osr1_end_RP1 (RP2)	TGGCTTTGATCATTCTGGGGC
	GFP_66_RP (FP2)	GTCGCCGTCCAGCTCGACCA

Click here to download Table S1

Table S2. Sequence of guide RNAs (gRNAs).

Name	Sequence (5' – 3')
mbait gRNA	CCACCTCTGGAACCGCAGCAGCC
col10a1 gRNA	CCACTGCACTTTCTCTGGGTTCC
osr1 gRNA	TGACACACGTTTGCTGAGCGCGG
col2a1a gRNA	AACATCCCGCCTGCCAATCGTGG

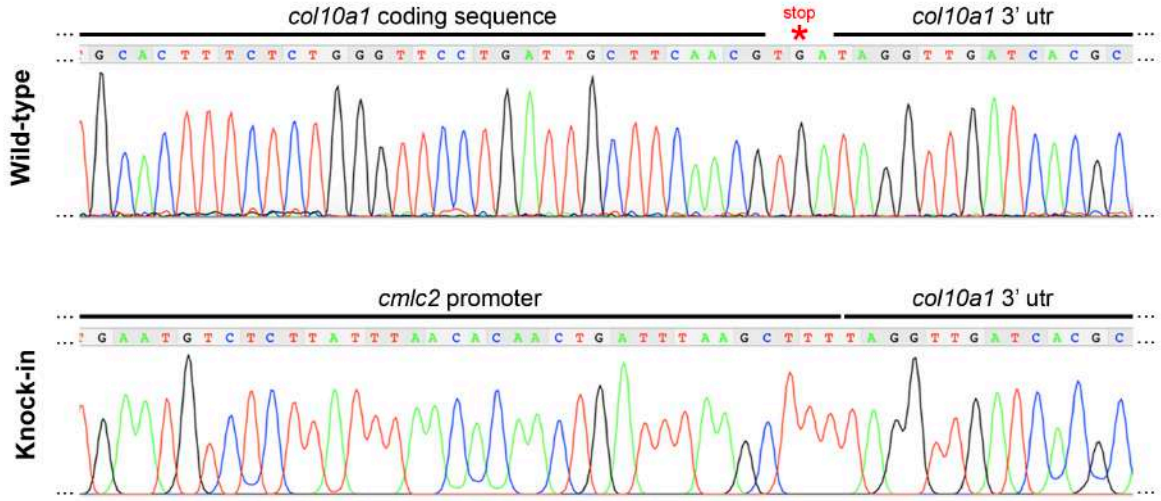

Fig. S1. DNA sequencing confirms precise knock-in at the 3' homology region in *col10a1*$^{p2a\text{-}CreERT2}$ medaka. In *col10a1*$^{p2a\text{-}CreERT2}$ medaka, *cmlc2* promoter sequence begins immediately upstream of the *col10a1* 3' untranslated region (utr).

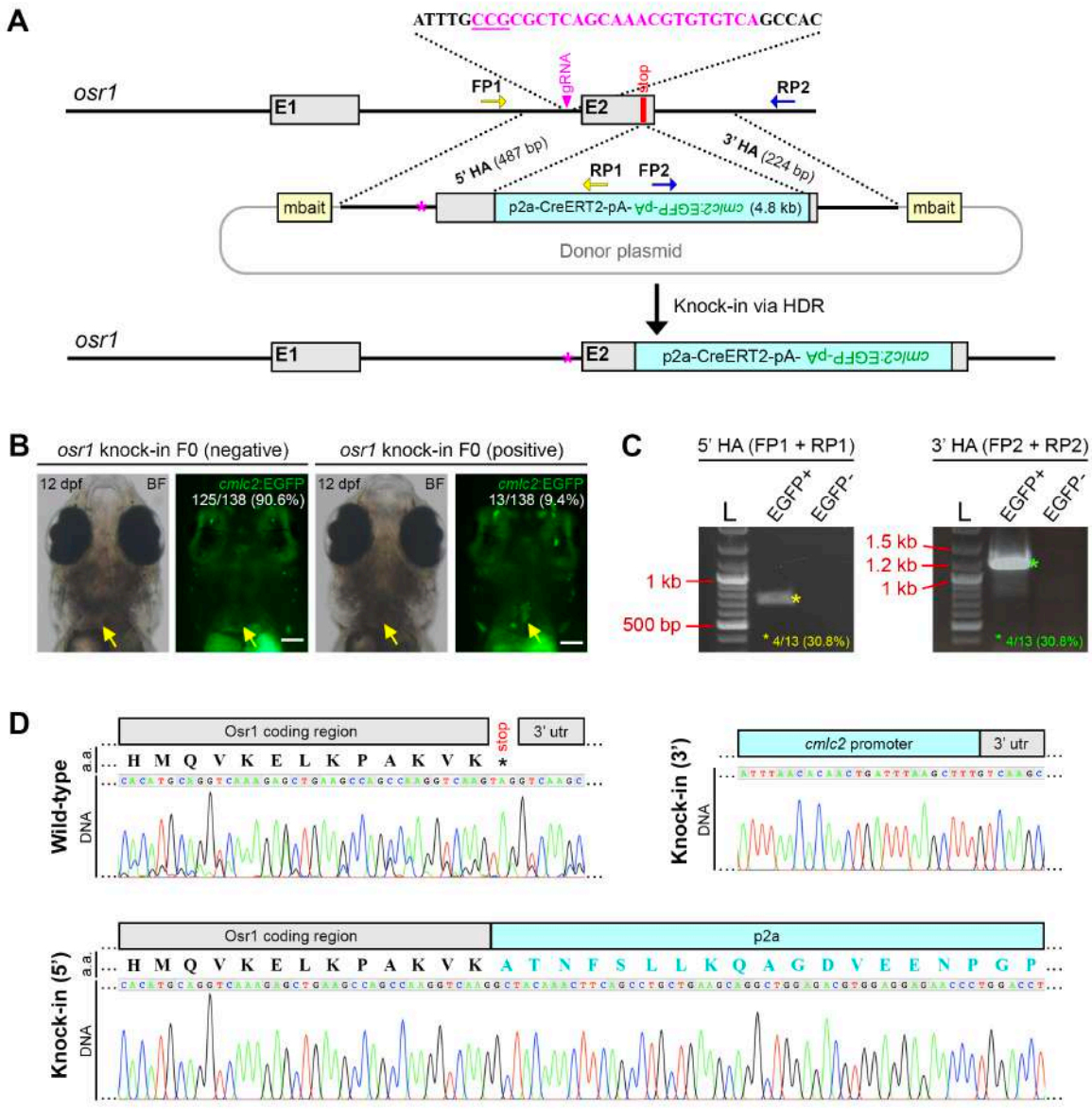

Fig. S2. Knock-in of p2a-CreERT2;*cmlc2*:EGFP into the medaka *osr1* locus using CRISPR/Cas9 and homology-directed repair (HDR).

A. Strategy for knock-in of p2a-CreERT2;*cmlc2*:EGFP into the *osr1* locus. A gRNA targeting *osr1* (indicated in magenta; PAM sequence underlined) was designed. A donor plasmid containing two mbait gRNA sites (yellow boxes) and two *osr1* homology arms (5' HA and 3' HA, 487 bp and 224 bp, respectively) flanking the p2a-CreERT2;*cmlc2*:EGFP sequence was used. Magenta asterisks indicate wobble bases incorporated at the *osr1* gRNA site. The endogenous *osr1* stop codon is indicated in red. Yellow arrows (FP1, RP1) and blue arrows (FP2, RP2) indicate primer pairs used for identification of precise knock-in at the 5' HA and 3' HA, respectively. **B.** Stereomicroscope fluorescent images showing *osr1* knock-in injected embryos (F0) with no

cmlc2:EGFP expression (left panel, yellow arrows; 125 out of 138 injected embryos) or mosaic *cmlc2*:EGFP expression (right panel, yellow arrows; 13 out of 138 injected embryos) in the heart. Scale bars: 100 µm. **C.** DNA agarose gel images showing PCR-genotyping of *cmlc2*:EGFP-positive (EGFP+) and *cmlc2*:EGFP-negative (EGFP-) larvae (F0) using the primer pairs as indicated in A. Yellow and green asterisks indicate the expected 712 bp and 1.2 kb, respectively. L, DNA ladder. Expected bands at the 5' and 3' homology regions were observed in 4 out of 13 EGFP+ larvae (30.8%). **D.** DNA sequencing of the 5' and 3' bands as shown in C (yellow and green asterisks, respectively) revealed precise knock-in at the *osr1* locus. Black asterisk indicates the endogenous *osr1* stop codon. a.a., amino acid.

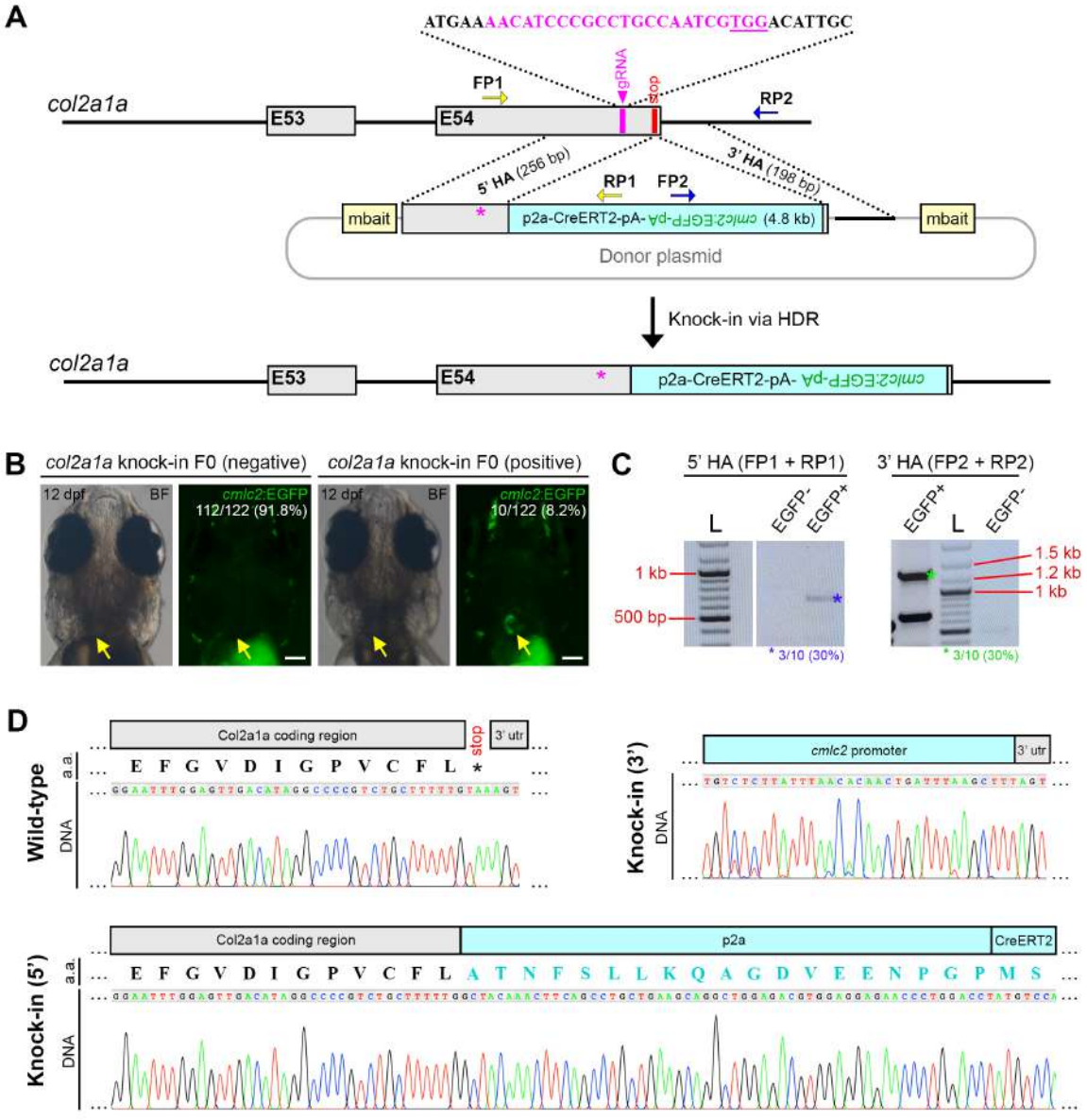

Fig. S3. Knock-in of p2a-CreERT2;*cmlc2*:EGFP into the medaka *col2a1a* locus using CRISPR/Cas9 and homology-directed repair (HDR).

A. For knock-in of p2a-CreERT2;*cmlc2*:EGFP into the *col2a1a* locus, a gRNA targeting *col2a1a* (indicated in magenta; PAM sequence underlined) was designed. A donor plasmid containing two mbait gRNA sites (yellow boxes) and two *col2a1a* homology arms (5' HA and 3' HA, 256 bp and 198 bp, respectively) flanking the p2a-CreERT2;*cmlc2*:EGFP sequence was used. Magenta asterisks indicate wobble bases incorporated at the *col2a1a* gRNA site. The endogenous *col2a1a* stop codon is indicated in red. Yellow arrows (FP1, RP1) and blue arrows (FP2, RP2) indicate primer pairs used for identification of precise knock-in at the 5' HA and 3' HA, respectively. **B.** Stereomicroscope fluorescent images showing *col2a1a* knock-in injected embryos with no *cmlc2*:EGFP expression (left panel, yellow arrows; 112 out of 122 injected embryos) or mosaic *cmlc2*:EGFP expression (right panel, yellow arrows; 10 out of 122 injected embryos) in the heart. Scale bars: 100 µm. **C.** DNA agarose gel images showing PCR-genotyping of *cmlc2*:EGFP-positive (EGFP+) and *cmlc2*:EGFP-negative (EGFP-) larvae (F0) using the primer pairs as indicated in A. Blue and green asterisks indicate the expected 612 bp and 1279 bp, respectively. L, DNA ladder. Expected bands at the 5' and 3' homology regions were observed in 3 out of 10 EGFP+ larvae (30%). **D.** DNA sequencing of the 5' and 3' bands as shown in C (blue and green asterisks, respectively) revealed precise knock-in at the *col2a1a* locus. Black asterisk indicates the endogenous *osr1* stop codon. a.a., amino acid.

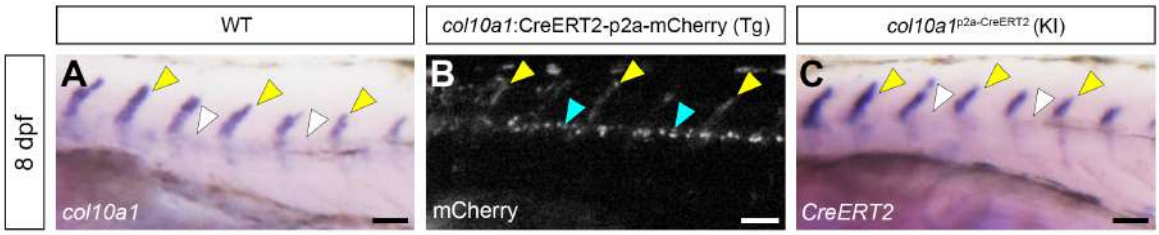

Fig. S4. Expression of endogenous *col10a1*, transgenic *col10a1*:CreERT2-p2a-mCherry and *CreERT2* in the *col10a1*$^{p2a\text{-}CreERT2}$ knock-in line at the medaka vertebral column. Lateral view of the 8 dpf medaka trunk showing whole-mount RNA *in situ* hybridization (WISH) of *col10a1* in wild-type (WT) medaka (A), mCherry fluorescence in *col10a1*:CreERT2-p2a-mCherry transgenic (Tg) medaka (B) and WISH of *CreERT2* in *col10a1*$^{p2a\text{-}CreERT2}$ knock-in (KI) medaka (C). Yellow arrows in A-C indicate expression in neural arches. Cyan arrows in B indicate expression in spinal cord neurons. White arrows in A, C indicate absence of expression in spinal cord neurons. Scale bars: 50 μm.

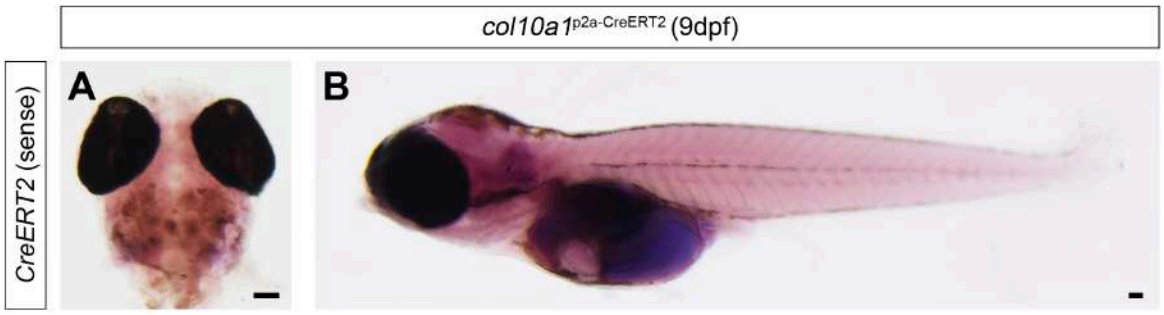

Fig. S5. Whole-mount RNA *in situ* hybridization using *CreERT2* sense riboprobes on 9 dpf *col10a1*$^{p2a\text{-}CreERT2}$ larvae. No specific staining was observed in the head (A, ventral view), trunk and caudal fin (B, lateral view). Scale bars: 100 µm.

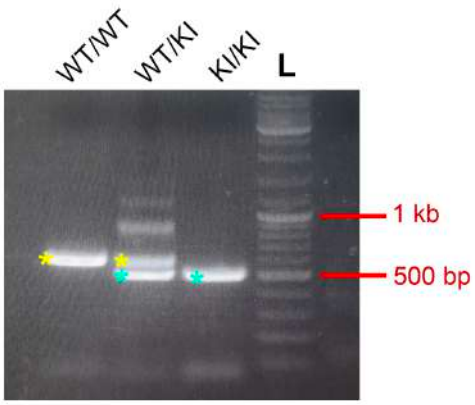

Fig. S6. DNA agarose gel showing genotyping of heterozygous *col10a1*$^{p2a\text{-}CreERT2}$ (WT/KI), homozygous *col10a1*$^{p2a\text{-}CreERT2}$ (KI/KI) and a wild-type sibling (WT/WT). Genotyping was performed via PCR using the primers indicated in Fig. 1 (FP1, RP1 and RP2). For WT/WT, a single 596 bp band was observed (yellow asterisk on the first lane). For KI/KI, a single 505 bp band was observed (cyan asterisk on the third lane). For WT/KI, both the 596 and 505 bp bands were observed (yellow and cyan asterisks, respectively). L, DNA ladder.

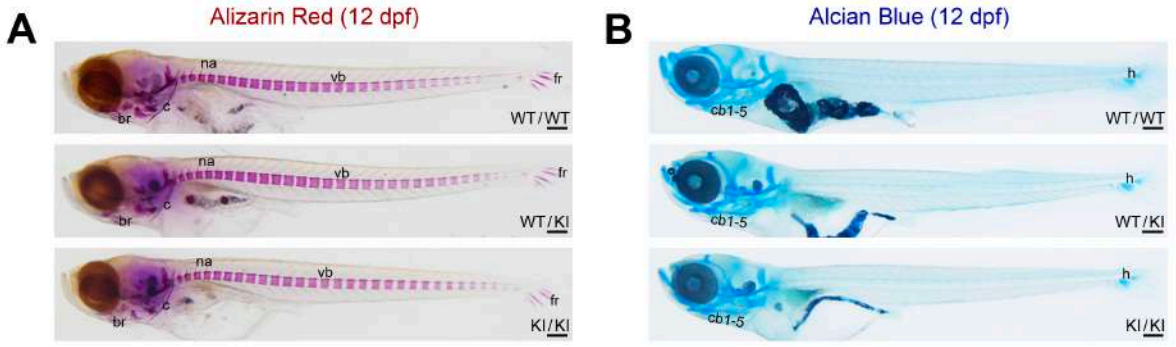

Fig. S7. Alizarin Red bone staining and Alcian Blue cartilage staining on 12 dpf heterozygous *col10a1*$^{p2a\text{-}CreERT2}$ (WT/KI), homozygous *col10a1*$^{p2a\text{-}CreERT2}$ (KI/KI) and WT siblings (WT/WT). Bone (A) and cartilage (B) formation were normal in WT/KI and KI/KI larvae compared to WT/WT controls. Images show the lateral view. br, branchiostegal ray. cb1-5, ceratobranchials 1-5. c, cleithrum. fr, fin ray. h, hypural. na, neural arch. vb, vertebral body. Scale bars: 200 µm.

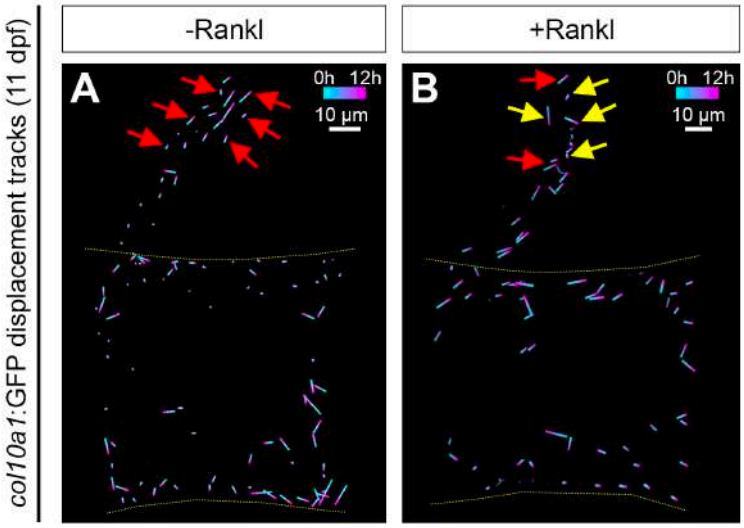

Fig. S8. Displacement tracks of *col10a*1:GFP cells in a vertebra of the vertebral column in non-Rankl and Rankl-induced conditions at 11 dpf. Tracks were generated from a 12 h time-lapse videos at 11 dpf in the absence of Rankl induction (A) or 2 days after Rankl induction (B). Yellow dotted lines demarcate the vertebral body. Arrows indicate *col10a1*:GFP cells at the neural arch. Yellow arrows indicate cells migrating ventrally (towards the vertebral body). Red arrows indicate cells migrating dorsally (away from the vertebral body). Scale bar: 10 µm.

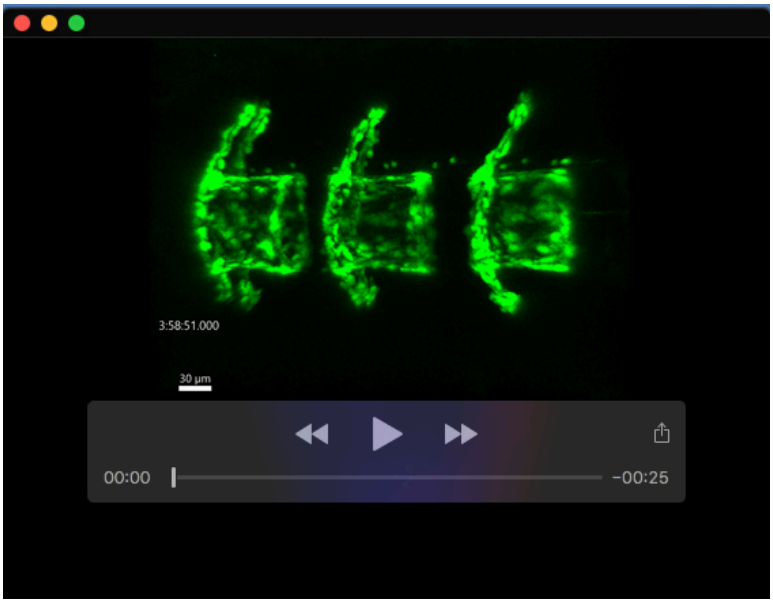

Movie 1. Time-lapse video showing *col10a*1:GFP osteoblast progenitors in medaka vertebral column beginning at 11 dpf. Time-lapse duration: 12 hours. Scale bar: 30 µm.